การศึกษาเพื่อเปรียบเทียบคุณสมบัติด้านฟิสิกส์และปริมาณรังสีระหว่างเครื่องเอกซเรย์คอมพิวเตอร์ที่ใช้ในงานรังสีวิทยาวินิจฉัยและงานรังสีรักษา

นางสาวนลพรรษ วงแหวน

วิทยานิพนธ์นี้เป็นส่วนหนึ่งของการศึกษาตามหลักสูตรปริญญาวิทยาศาสตรมหาบัณฑิต

สาขาวิชาฉายาเวชศาสตร์ ภาควิชารังสีวิทยา

คณะแพทยศาสตร์ จุฬาลงกรณ์มหาวิทยาลัย

ปีการศึกษา 2548

ISBN 974-53-2584-8

COMPARATIVE STUDY IN PHYSICAL PERFORMANCE AND DOSIMETRIC CHARACTERIZATION BETWEEN DIAGNOSTIC AND THERAPEUTIC CT SCANNERS

Miss Nonlapas Wongwaen

A Thesis Submitted in Partial Fulfillment of the Requirements for the Degree of Master of Science Program in Medical Imaging

Department of Radiology
Faculty of Medicine
Chulalongkorn University

Academic Year 2005

ISBN 974-53-2584-8

Title	Comparative Study in Physical Performance and Dosimetric Characterization between Diagnostic and Therapeutic CT Scanners
By	Miss Nonlapas Wongwaen
Field of study	Medical Imaging
Thesis advisor	Associate Professor Sivalee Suriyapee
Thesis co-advisor	Mr. Taweap Sanghangthum

Accepted by the Faculty of Medicine, Chulalongkorn University in partial fulfillment of the requirement for Master's Degree

P. Kamolratanakul .... Dean of the Faculty of Medicine
(Professor Pirom Kamol-ratanakul, M.D., M.Sc.)

THESIS COMMITTEE :

Somjai Wangsuphachart .... Chairman
(Associate Professor Somjai Wangsuphachart, M.D., M.Sc.)

Sivalee Suriyapee .... Thesis Advisor
(Associate Professor Sivalee Suriyapee, M.Eng.)

Taweap Sanghangthum .... Thesis Co-Advisor
(Mr. Taweap Sanghangthum, M.Sc.)

.... Member
(Assistant Professor Sukalaya Lerdlum, M.D., M.Sc.)

Weeranuch Kitsukjit .... Member
(Mrs. Weeranuch Kitsukjit, M.Sc.)

นางสาวนลพรรษ วงแหวน : การศึกษาเพื่อเปรียบเทียบคุณสมบัติด้านฟิสิกส์และปริมาณรังสีระหว่างเครื่องเอกซเรย์คอมพิวเตอร์ที่ใช้ในงานรังสีวิทยาวินิจฉัยและงานรังสีรักษา. (COMPARATIVE STUDY IN PHYSICAL PERFORMANCE AND DOSIMETRIC CHARACTERIZATION BETWEEN DIAGNOSTIC AND THERAPEUTIC CT SCANNERS). อาจารย์ที่ปรึกษา : รศ. ศิวลี สุริยาปี, อาจารย์ที่ปรึกษาร่วม : นายทวีป แสงแห่งธรรม ; 75 หน้า ISBN 974-53-2584-8

เครื่องจำลองการฉายรังสีเอกซเรย์คอมพิวเตอร์นำมาใช้สร้างภาพสามมิติเพื่อคำนวณการกระจายรังสี ซอฟแวร์ของเครื่องจำลองการฉายรังสีดังกล่าวช่วยในการวางลำรังสี และการออกแบบการรักษา เครื่องเอกซเรย์คอมพิวเตอร์ต้องการให้มีเส้นผ่านศูนย์กลางของโพรงขนาดใหญ่ เพื่อให้ผู้ป่วยสามารถอยู่ในท่าเดียวกับการฉายรังสี วัตถุประสงค์ในการศึกษางานวิจัยนี้ เพื่อประเมินคุณสมบัติด้านฟิสิกส์และปริมาณรังสีของเครื่องเอกซเรย์คอมพิวเตอร์ที่ใช้ในงานรังสีรักษา และเปรียบเทียบกับเครื่องเอกซเรย์คอมพิวเตอร์ทางรังสีวินิจฉัย เมื่อเลือกปัจจัยต่างๆให้เหมือนกัน

คุณภาพของภาพของเครื่องเอกซเรย์คอมพิวเตอร์ที่มีเส้นผ่านศูนย์กลางของโพรงขนาด 80 ซ.ม. (GE LightSpeed RT) และเครื่องที่มีเส้นผ่านศูนย์กลางของโพรงขนาด 70 ซ.ม. ที่ใช้ในงานรังสีวินิจฉัย (GE LightSpeed Plus®) แสดงโดยใช้หุ่นจำลองของบริษัท และหุ่นจำลองแคทแฟน ซึ่งเป็นหุ่นจำลองอิสระ (CATPHAN 500) ปัจจัยที่ทำการศึกษาได้แก่ ความเที่ยงตรงของความหนาของสไลซ์ ความเที่ยงตรงและภาวะเชิงเส้นของเลขซีที ความสม่ำเสมอของเลขซีทีและสัญญาณรบกวน การแสดงรายละเอียดด้านความคมชัดต่ำ การแสดงรายละเอียดด้านความคมชัดสูง และปริมาณรังสีวัดโดยใช้วิธีการที่เป็นมาตรฐานในการวัดศีรษะและลำตัว

หุ่นจำลองแคทแฟนเป็นอุปกรณ์มาตรฐาน ที่ใช้ในการเปรียบเทียบคุณภาพของเครื่องเอกซเรย์คอมพิวเตอร์ทั้ง 2 เครื่อง ผลการศึกษาในครั้งนี้แสดงว่า ทั้ง 2 เครื่องมีคุณภาพไม่ได้แตกต่างกันอย่างมีนัยสำคัญ ความหนาของสไลซ์อยู่ภายในค่าเกณฑ์ที่ยอมรับได้คือ ± 0.5 มม. การเปรียบเทียบเรื่อง ความเที่ยงตรง ภาวะเชิงเส้น และความสม่ำเสมอของเลขซีที มีความใกล้เคียงกัน คอนทราสต์สเกลของเครื่อง LightSpeed Plus® และ LightSpeed RT คือ 1.92×10^{-4} ซม.$^{-1}$/เลขซีที และ 1.91×10^{-4} ซม.$^{-1}$/เลขซีที ตามลำดับ เครื่องที่มีโพรง 80 ซม. มีสัญญาณรบกวนเพิ่มขึ้นเล็กน้อย เมื่อเปรียบเทียบกับเครื่องที่มีโพรง 70 ซม. ที่ความคมชัด 0.3% เครื่อง LightSpeed Plus® และ LightSpeed RT สามารถแยกวัตถุที่มีขนาด 8 มม.และ 9 มม. ออกจากพื้นหลังได้ ตามลำดับ ที่ 5% ของ MTF LightSpeed Plus® และ LightSpeed RT สามารถแยกวัตถุที่มีขนาด 7.14 เส้นคู่/ซม. และ 7.29 เส้นคู่/ซม. ออกจากกันได้ ตามลำดับ เครื่อง LightSpeed RT มีการแสดงรายละเอียดด้านความคมชัดสูงเพิ่มมากขึ้น แต่ การแสดงรายละเอียดด้านความคมชัดต่ำลดลง เปอร์เซ็นต์นอยส์เพิ่มขึ้น และปริมาณรังสีลดลงเมื่อเปรียบเทียบกับเครื่อง LightSpeed Plus® ผลการศึกษาที่ได้จากหุ่นจำลองบริษัทสอดคล้องกับหุ่นจำลองแคทแฟน และมีความเชื่อถือในการใช้ตรวจสอบเครื่องประจำวันได้ เครื่อง LightSpeed RT มีคุณภาพบรรลุตามวัตถุประสงค์ของการเป็นเครื่องจำลองการฉายรังสีคือ สร้างภาพรังสีที่มีคุณภาพสูงและมีความเที่ยงตรง

ภาควิชา รังสีวิทยา ลายมือชื่อนิสิต นลพรรษ วงแหวน

สาขาวิชา ฉายาเวชศาสตร์ ลายมือชื่ออาจารย์ที่ปรึกษา ศิวลี สุริยาปี

ปีการศึกษา 2548 ลายมือชื่ออาจารย์ที่ปรึกษาร่วม ทวีป แสงแห่งธรรม

4774739130: MAJOR MEDICAL IMAGING

KEYWORDS: MULTI-SLICE CT / CT RADIATION EXPOSURE / CT IMAGE QUALITY/ CT SIMULATOR

NONLAPAS WONGWAEN: COMPARATIVE STUDY IN PHYSICAL PERFORMANCE AND DOSIMETRIC CHARACTERIZATION BETWEEN DIAGNOSTIC AND THERAPEUTIC CT SCANNERS. THESIS ADVISOR : ASSOC. PROF. SIVALEE SURIYAPEE, THESIS CO- ADVISOR : MR. TAWEAP SANGHANGTHUM.75 pp. ISBN 974-53-2584-8

CT simulator is used to acquire a volumetric image for dose distribution calculation. With virtual simulation software, beam placement and treatment design could be performed. The therapeutic CT simulation process required large gantry bore to simulate all patients in a comfortable treatment position. The purpose of this study is to evaluate the physical performance and dosimetric characterization of large-bore CT simulator and compare with the diagnostic CT scanner in the same setting.

The image quality of an 80 cm bore CT scanner (GE LightSpeed RT) and a 70 cm bore diagnostic type scanner (GE LightSpeed Plus®) were performed using manufacturer QA phantom and independent image quality phantom (CATPHAN 500). The evaluated parameters were; slice thickness accuracy, CT number accuracy and linearity, uniformity and noise, low contrast resolution, and high contrast resolution. The computed tomography dose index was measured in phantom for standard head and body imaging protocols.

The measurement with CATPHAN phantom is the standard tool to compare the quality of both scanners. The result showed no significantly difference for the quality of both units. Measured slice thickness was within acceptable criteria of $\pm$ 0.5 mm. Both units exhibited comparable CT number accuracy, linearity and uniformity. The contrast scales were $1.92\times10^{-4}cm^{-1}$/CT no. for LightSpeed Plus® and $1.91\times10^{-4}cm^{-1}$/CT no. for LightSpeed RT. The 80 cm bore scanner showed slightly increased in noise compared to 70 cm bore scanner. For low-contrast resolution, LightSpeed Plus® obtained 8 mm at 0.3% contrast compared to 9 mm at the same contrast for LightSpeed RT. For high contrast scale, LightSpeed Plus® showed 7.14 lp/cm compare to 7.29 lp/cm at 5% MTF for LightSpeed RT. The results showed that LightSpeed RT gave slightly increased high contrast resolution but slightly decreased in low-contrast resolution, the percent noise was higher and the radiation dose was lower when compared with LightSpeed Plus®. The results from manufacturer QA phantom agree with CATPHAN phantom and proved to be reliable for routine constancy check. The LightSpeed RT was a successful CT-simulation process, the CT-scanner consistently produced patient images with the highest possible quality and accurate geometrical information.

Department.........Radiology.........Student's signature. Nonlapas Wongwaen

Field of study.......Medical Imaging.....Advisor's signature. Sivalee Suriyapee

Academic year.........2005.........Co-advisor's signature. Taweap Sanghangthum

ACKNOWLEDGEMENTS

I would like to express gratitude and deepest appreciation to Associate Professor Sivalee Suriyapee, Chief Physicist at Division of Radiation Oncology, Department of Radiology, Faculty of Medicine, Chulalongkorn University, my major advisor for her guidance, invaluable advice, supervision, constructive comments and English language proof in this research. I am equally grateful to Mr. Taweap Sanghangthum, Physicist at Division of Radiation Oncology, Department of Radiology, King Chulalongkorn Memorial Hospital, my co-advisor for his help in the experiment, kind suggestion and constructive comments in the experiments.

I would like to deeply thank Associate Professor Somjai Wangsuphachart, Chief of Department of Radiology, Faculty of Medicine, Chulalongkorn University for great advice and all comments for my research.

I would like to deeply thank my thesis committee, Assistant Professor Sukalaya Lerdlum, Head of Diagnostic Division, Department of Radiology, Faculty of Medicine, Chulalongkorn University and Mrs. Weeranuch Kitsukjit for her kindness in examining the research methodology and provide suggestions for the improvement.

I would like to deeply thank Associate Professor Anchali Krisanachinda, Director of Division of Nuclear Medicine, Department of Radiology, Faculty of Medicine, Chulalongkorn University for in valuable advice, constructive comments and English language proof in this research.

I would like to deeply thank a captain in the air force Piyanat Kamonchot, Bhumibol- adulyadej Hospital (Thai Air Force Hospital), Director, for the permission to use the diagnostic device in this research and a commander in the air force Suntorn Lekburut ,Technician of Department of Radiology, Bhumibol- adulyadej Hospital for his providing the comfortable workshop, the convenient measurement and suggestion for the use of the device.

I am grateful to all teachers, lecturers and staff in Master Science Program in Medical Imaging, Faculty of Medicine, Chulalongkorn University for their kind support and supply the knowledge in Medical Imaging, especially Dr. Napapong Pongnapang, Dr. Saowapak Sotthivirat and Mr. Sornjarod Oonsiri.

Finally, I am grateful to my family for their financial support, valuable encouragement, entirely care and understanding during the entire course of study.

CONTENTS

CHAPTER **Page**

CHAPTER **Page**

CHAPTER **Page**

CHAPTER **Page**

LIST OF TABLES

Table **Page**

LIST OF FIGURES

Figure **Page**

Figure **Page**

ABBREVIATION

Abbreviation	Terms
AAPM	American Association of Physicists in Medicine
cGy	Centigray
cm	Centimeter
CRT	Conformal Radiation Therapy
CT	Computed Tomography
CTDI	Computed Tomography Dose Index
$CTDI_{100}$	Computed Tomography Dose Index at 100 mm
$CTDI_w$	Computed Tomography Dose Index Weighted
CT no.	Computed Tomography Number
DAS	Data Acquisition System
DFOV	Display Field of View
FWHM	Full Width at Half Maximum
HQ	High Quality
HS	High Speed
HU	Hounsfield Units
HVL	Half Value Layer
IMRT	Intensity - Modulated Radiation Therapy
keV	Kilo Electron Volt
kV	Kilovoltage
kVp	Kilovoltage Peak
LCD	Low Contrast Detectability

Abbreviation	Terms
lp/cm	Linepair per Centimeter
LSF	Line Spread Function
mA	Milliampere
mAs	Milliampere-second
MHU	Mega Heat Unit
mm	Millimeter
MTF	Modulation Transfer Function
PSF	Point Spread Function
QA	Quality Assurance
ROI	Region of Interest
s	Second
S0mm, S40mm, S60mm	Superior 0, 40,60 millimeters
SFOV	Scan Field of View
SMPTE	Society of Motion Picture and Television Engineers
vs.	Versus

CHAPTER I

INTRODUCTION

The goal of radiation therapy (RT) is to deliver a therapeutic dose of radiation to the tumor without damaging surrounding healthy tissues. Delivery of a curable radiation dose is limited, however, by normal tissue tolerance, necessitating the move toward more precise 3D dose delivery with techniques such as 3D conformal radiation therapy (3DCRT) or intensity-modulated RT (IMRT). These techniques provide a more effective means of achieving improved tumor coverage with a therapeutic dose of radiation while maintaining normal tissue complications at a minimum. These improvements in RT have been made possible by advances in volumetric-based image planning with digital imaging systems such as computed tomography (CT), together with the standardization of guidelines for defining tumor volume.

CT for radiotherapy, the demand for CT virtual simulation is constantly increasing, planning or CT simulation involves the acquisition of a CT image data set of the patient and the subsequent treatment simulation using sophisticated virtual beam displays in three dimensions based on digitally reconstructed radiographs. CT simulation systems can reconstruct images in any plane and can generate volume-rendered displays that allow for improved perspective of tumor and normal tissues, necessary for the delineation of the tighter margins around the clinical target volume as defined by 3DCRT and IMRT. Due to the escalation in radiation dose permitted by these techniques, superior CT image quality is critical for accurate delineation of the tumor volume and critical tissue structures to ensure complete tumor destruction and healthy tissues preservation.

Virtual simulation CT studies are typically acquired on conventional diagnostic scanners equipped with an external patient positioning laser system and specialized planning and virtualization software. Virtual simulation technology has matured to point where conventional simulators may be replaced with CT scanners. However, diagnostic CT scanner gantry bores can present an obstacle to the CT simulation process by limiting patient positions, compared to those that can be attained in a conventional simulator. For example, breast cancer patients cannot always be scanned in the treatment position without compromising reproducibility and appropriateness of setup. Extremely large patients or patients requiring special immobilization or large setup devices are often unable to enter the limited-bore gantry. A therapeutic CT simulation scanner has the potential to eliminate these problems.

The performance and dosimetric characterization of CT scanner were studied and reported in some literatures but there is no study of large-bore multi-slice CT scanner. The importance of superior image quality required of volumetric-based, escalated-dose radiotherapy techniques motivated us to characterize and evaluate the image quality of the CT simulation scanners available in Department of Radiology, King Chulalongkorn Memorial Hospital. In 2004, the first of CT simulator large–bore scanner is installed in Thailand. Fortunately, the diagnostic scanner of 70-cm bore

LightSpeed Plus® was installed in Bhumibol-adulyadej Hospital and the permission was allowed to study the quality of the image compare with the large bore.

The purpose of this study is to evaluate the physical performance in image quality and dosimetric characterization of large-bore CT simulator and compare with the diagnostic CT scanner in the same setting. According to AAPM No. 39 [1], AAPM Summer school 1995 [2], AAPM – TG66 Report [3], or manual suggested, [4, 5] quality control of CT image quality includes the evaluation of image slice thickness (or slice sensitivity profile), CT number accuracy and linearity, image uniformity and noise, low-contrast detectability (LCD), and high contrast resolution. In this study, the performance of CT scanner was checked by the manufacturer phantom to assure the accuracy and reproducibility of the machine. The CATPHAN phantom is used to evaluate the physical performance of both scanners. Another important aspect for CT scanners is the patient dose. Although this parameter dose not provide information on image quality directly, dosimetry (CT dose index, CTDI) is important for the determination of radiation dose delivered to the patient. CTDI was determined in head and body phantoms and is included in this report.

CHAPTER II

REVIEW OF RELATED LITERATURES

Jose L. et al [6] studied the performance of an 85-cm-bore CT X-ray scanner designed specifically for radiation oncology and compared it against diagnostic-type, 70-cm-bore scanner that may be used in the same setting. Both are single-slice helical CT. They performed image quality and dosimetric measurements on an 85-cm-bore CT scanner (AcQsim) and a 70-cm-bore, diagnostic-type scanner (UltraZ). Image quality measurements were performed using a manufacturer-supplied phantom, and an independent image quality phantom (CATPHAN). The standard image quality parameters evaluated for the purpose of comparison were as follows: slice thickness accuracy, high-contrast resolution (limiting spatial resolution), low-contrast resolution, uniformity and noise, and CT number accuracy and linearity. The computed tomography dose index was measured for standard head and body imaging protocols using accepted methods and procedures. For comparison purposes, data for a diagnostic-type, 70-cm-bore scanner (GE HighSpeed CT/i) were extracted from the literature. The results were following: head and body doses seem on average to be slightly (1 – 2 cGy) higher for the 85-cm-bore unit than for conventional 70-cm-bore unit, measured slice thickness was within acceptable criteria (±0.5 mm). There does not seem to be any significant difference in high-contrast resolution. Both units render a limiting value of ~7-8 lp/cm for slice thickness 8-10 mm. Both units exhibit comparable CT number uniformity accuracy and linearity. Noise levels seem to be slightly increased (by ~0.05-0.2%) for the large-bore geometry. Low-contrast resolution for both units was comparable (4.5-5.5 mm @ 0.35%). All image quality parameters are well within diagnostic acceptable levels.

McCollough C.H, and Zink F.E, [7] studied about the performance of a multi slice CT scanner (LightSpeed QX/i) in comparison to a single-slice CT scanner from the same manufacturer (HiSpeed CT/i). Pitch is refined definition, yet maintains the existing relationship between pitch, patient dose, and image quality. The following performance parameters were assessed: radiation and slice sensitivity profiles, low-contrast and limiting spatial resolution, image uniformity and noise, CT number and geometric accuracy, and dose. The multi-slice system was tested in axial (1, 2, or 4 images per gantry rotation) and HQ (Pitch = 0.75) and HS (Pitch = 1.5) helical modes. Axial and helical acquisition speed and limiting spatial resolution
(0.8 s exposure) were improved on the multi-slice system. Slice sensitivity profiles, image noise, CT number accuracy and uniformity, and low-contrast resolution were similar. In some HS-helical modes, helical artifacts and geometric distortion were more pronounced with a different appearance. Radiation slice profiles and dose were large on the multi-slice system at all scan widths. For a typical abdomen and pelvis exam, the central and surface body doses for 5-mm helical scans were higher on the multi-slice system by approximately 50%. The increase in surface CTDI values (with respect to the single-slice system) was greatest for the 4×1.25-mm detector configuration (190% for head 240% for body) and least for the 4×5-mm configuration (53% for head, 76% for body). Preliminary testing of version 1.1 software demonstrated reduced doses on the multi-slice scanner, where the increase in body

surface CTDI values (with respect to the single-slice system) was 105% for the 4×1.25-mm detector configuration and 10% for the 4×5-mm configuration. In summary, the axial and HQ-helical modes of the multi-slice system provided excellent image quality and a substantial reduction in exam time and tube loading, although at varying degrees of increased dose relative to the single-slice scanner.

McCann C. and Alasti H. [8] evaluated and compared the image quality of three unique CT simulation scanners available at their center, Princess Margaret Hospital in Toronto, Canada, for both single -slice and multiple-slice helical scanners. These scanners included a conventional 70-cm bore single-slice scanner (Phillips), a large 85-cm bore single scanner (Phillips), and a 70-cm bore multi-slice scanner (GE). Image quality was evaluated in terms of image noise, low-contrast detectability (LCD), limiting spatial resolution (modulation transfer function), and slice thickness accuracy in accordance with guidelines set out by the AAPM. A commercially available CATPHAN phantom was used to characterize image quality for both axial and helical modes of scanning. They found that image quality was generally comparable for all scanners. Limiting spatial resolution and slice thickness accuracy were comparable for all three scanners for both scanning modes. The multi-slice unit was superior in terms of noise content, resulting in improved visualization of small, low-contrast objects. In addition, the multi-slice unit optimizes volume coverage speed and longitudinal resolution without compromising image quality, a significant advantage for the radiation oncology environment.

Jangsri N. [9] studied an evaluation of spatial resolution in computerized tomography. This research presented the methods of spatial resolution measurement for FWHM and MTF in CT scanner with accuracy and efficiency without the used of special software. CATPHAN phantom was used to measure spatial resolution in 11 CT scanners. The method fits the measured point spread function (PSF) data with a Gaussian function that has a single value of the spatial resolution of the CT units. The characteristic parameter is related to FWHM of the PSF. The characteristic parameter for the Gaussian fitted to the PSF data is obtained by plotting $\sqrt{\ln\left(\frac{1}{\mathrm{PSF}}\right)}$ versus the radial distance (r). The slope of the resulting linear regression fitted to the data yields the value of α. The characteristic parameter,

$$\alpha = \frac{1.665}{\mathrm{FWHM}} \qquad [2.1]$$

, provides a single number by means of which the spatial resolution of CT scanners can be monitored easily. The method assumes radial symmetry for the PSF. The MTF of a Gaussian PSF is also Gaussian in form. Hence, once the PSF is fitted with a Gaussian function, the MTF can be directly determined by simple equation,

$$\mathrm{MTF}(\upsilon)=e^{-\left(\frac{\pi\upsilon}{10\alpha}\right)^{2}} \qquad [2.2]$$

Data taken from eleven different scanners illustrate that the Gaussian approximation to the PSF was reasonable; the correlation coefficient was greater than 0.99 in each scan. Furthermore, the standard Fourier transform computed MTF showed good agreement with the MTF obtained from the Gaussian PSF which are tested by Correlation and Student t-test showing the reliability of 99% (Correlation : $r > 0.99$, Student t-test : $p_{value} < 0.01$).

CHAPTER III

THEORY

3.1 Computed Tomography (CT)

3.1.1 Basic Principles [10]

The mathematical principles of CT were first developed by Radon in 1917. Radon’s treatise proved that an image of an unknown object could be produced if one had an infinite number of projections through the object. We can understand the basic idea behind tomographic imaging with an example taken from radiography.

With plain film imaging, the three-dimensional (3D) anatomy of the patient is reduced to a two-dimensional (2D) projection image. The density at a given point on an image represents the x-ray attenuation properties within the patient along a line between the x-ray focal spot and the point on the detector corresponding to the point on the image. Consequently, with a conventional radiograph of the patient’s anatomy, information with respect to the dimension parallel to the x-ray beam is lost. This limitation can be overcome, at least for obvious structures, by acquiring both a posteroanterior (PA) projection and a lateral projection of the patient. For example, the PA chest image yields information concerning height and width, integrated along the depth of the patient, and the lateral projection provides information about the height and depth of the patient, integrated over the width dimension (Fig. 3.1). For objects that can be identified in both images, such as a pulmonary nodule on PA and lateral chest radiographs, the two films provide valuable location information. For more complex or subtle pathology, however, the two projections are not sufficient. Imagine the instead of just two projections, a series of 360 radiographs were acquired at 1-degree angular intervals around the patient’s thoracic cavity. Such a set of images provides essentially the same data as a thoracic CT scan. However, the 360 radiographic images display the anatomic information in a way that would be impossible for a human to visualize: cross-sectional images. If these 360 images were stored into a computer, the computer could in principle reformat the data and generate a complete thoracic CT examination.

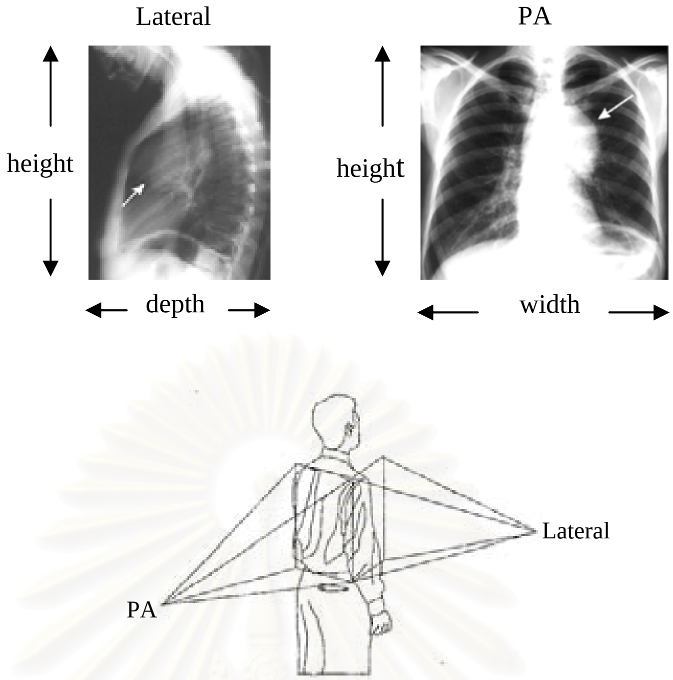

Figure 3.1 Posteroanterior and lateral chest radiographs

The tomographic image is a picture of a slap of the patient's anatomy. The 2D CT image corresponds to a 3D section of the patient, so that even with CT, three dimensions are compressed into two. However, unlike the case with plain film imaging, the CT slice-thickness is very thin (1 to 10 mm) and is approximately uniform. The 2D array of pixels (short for picture elements) in the CT image corresponds to an equal number of 3D voxels (volume elements) in the patient. Voxels have the same in-plane dimensions as pixels, but they also include the slice thickness dimension. Each pixel on the CT image displays the average x-ray attenuation properties of the tissue in the corresponding voxel (Fig. 3.2).

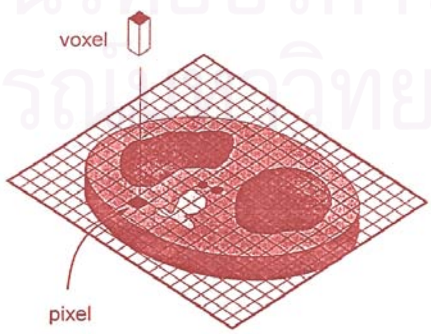

Figure 3.2 Pixel (picture element) and voxel (volume element) of a digital image

3.1.2 Tomographic Acquisition [10]

A single transmission measurement through the patient made by a single detector at a given moment in time is called a ray. A series of rays that pass through the patient at the same orientation is called a projection or view. There are two projection geometries that have been used in CT imaging (Fig. 3.3). The more basic type is parallel beam geometry, in which all of the rays in a projection are parallel to each other. In fan beam geometry, the rays at a given projection angle diverge and have the appearance of a fan. All modern CT scanners incorporate fan beam geometry in the acquisition and reconstruction process. The purpose of the CT scanner hardware is to acquire a large number of transmission measurements through the patient at different positions. The acquisition of a single axial CT image may involve approximately 800 rays taken at 1,000 different projection angles, for a total of approximately 800,000 transmission measurements. Before the axial acquisition of the next slice, the table that the patient is lying on is moved slightly in the cranial-caudal direction (the z-axis of the scan), which positions a different slice of tissue in the path of the x-ray beam for the acquisition of the next image.

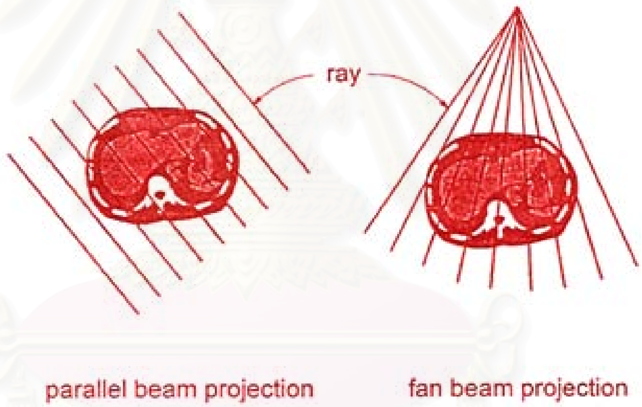

Figure 3.3 Two types of CT beam projection

3.1.3 Tomographic Reconstruction [10]

Each ray that is acquired in CT is a transmission measurement through the patient along a line, where the detector measures an x-ray intensity, I_t. The unattenuated intensity of the x-ray beam is also measured during the scan by a reference detector, and this detects an x-ray intensity I_0. The relationship between I_t and I_0 is given by

$$I_t = I_0 e^{-\mu t} \qquad [3.1]$$

Where t is the thickness of the patient along the ray and μ is the average linear attenuation coefficient along the ray. Notice that I_t and I_0 are machine-dependent values, but the product μt is an important parameter relating to the anatomy of the patient along a given ray. When the equation is rearranged, the measured values I_t and I_0 can be used to calculate the parameter of interest:

$$\ln\left(\frac{I_0}{I_t}\right) = \mu t \qquad [3.2]$$

Where ln is the natural logarithm (to base e, e = 2.78…), t ultimately cancels out, and the value μ for each ray is used in the CT reconstruction algorithm. This computation, which is a preprocessing step performed before image reconstruction, reduces the dependency of the CT image on the machine-dependent parameters, resulting in an image that depends primarily on the patient's anatomic characteristics. This is very much a desirable aspect of imaging in general, and the high clinical utility of CT results, in part, from this feature. By comparison, if it is overexposed (I_0 too high) it appears too dark. The density of CT images is independent of I_0, although the noise in the image is affected.

After preprocessing of the raw data, a CT reconstruction algorithm is used to produce the CT images. There are numerous reconstruction strategies; however, filtered back projection reconstruction is most widely used in clinical CT scanners. The back projection method builds up the CT image in the computer by essentially reversing the acquisition steps (Fig. 3.4). During acquisition, attenuation information along a known path of the narrow x-ray beam is integrated by a detector. During back projection reconstruction, the μ value for each ray is smeared along this same path in the image of the patient. As the data from a large number of rays are back projection onto the image matrix, areas of high attenuation tend to reinforce each other, and areas of low attenuation also reinforce, building up the image in the computer.

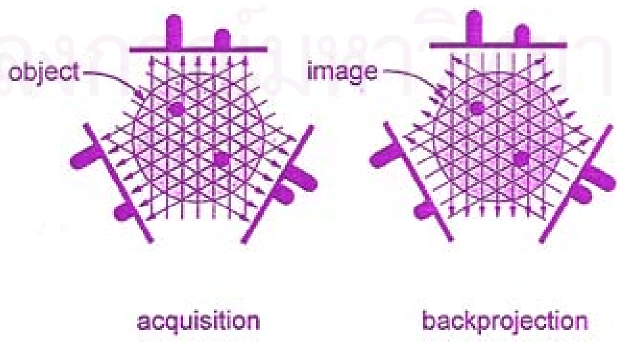

Figure 3.4 Data acquisition in computed tomography (CT)

3.1.4 CT Number or Hounsfield Units

After CT reconstruction, each pixel in the image is represented by a high-precision floating point number that is useful for computation but less useful for display. Most computer display hardware makes use of integer images. Consequently, after CT reconstruction, but before storing and displaying, CT images are normalized and truncated to integer values. The number *CT*(*x*,*y*) in each pixel, (*x*,*y*), of the image is converted using the expression 3.3:

$$CT(x,y) = 1{,}000 \times \frac{\mu(x,y) - \mu_{water}}{\mu_{water}} \quad [3.3]$$

where $\mu(x,y)$ is the floating point number of the (x,y) pixel before conversion, μ_{water} is the attenuation coefficient of water, and $CT(x,y)$ is the CT number (or Hounsfield Unit) that ends up in the final clinical CT image. The value of μ_{water} is about 0.195 for the x-ray beam energies typically used in CT scanning. This normalization results in CT numbers ranging from about -1,000 to +3,000, where -1,000 corresponds to air, soft tissues range from -300 to -100, water is 0, and dense bone and areas filled with contrast agent range up to +3,000.

CT images are produced with a highly filtered, high-kV x-ray beam, with an average energy of about 75 keV. At this energy in muscle tissue, about 91% of x-ray interactions are Compton scatter. For fat and bone, Compton scattering interactions are 94% and 74%, respectively. Therefore, CT numbers and hence CT images derive their contrast mainly from the physical properties of tissue that influence Compton scatter. Density (g/cm^3) is a very important discriminating property of tissue (especially in lung tissue, bone, and fat), and the linear attenuation coefficient, μ, tracks linearly with density. Other than physical density, the Compton scatter cross section depends on the electron density (ρ_e) in tissue: ρ_e= NZ/A, where N is Avogadro's number (6.023 × 10^{23}, a constant), Z is the atomic number, and A is the atomic mass of the tissue. The main constituents of soft tissue are hydrogen (Z = 1, A = 1), carbon (Z = 6, A = 12), nitrogen (Z =7, A = 14), and oxygen (Z = 8, A = 16). Carbon, nitrogen, and oxygen all have the same Z/A ratio of 0.5, so their electron densities are the same. Because the Z/A ratio for hydrogen is 1.0, the relative abundance of hydrogen in a tissue has some influence on CT number. Hydrogenous tissue such as fat is well visualized on CT. Nevertheless, density (g/cm^3) plays the dominant role in forming contrast in medical CT.

CT numbers are quantitative, and this property leads to more accurate diagnosis in some clinical settings. For example, pulmonary nodules that are calcified are typically benign, and the amount of calcification can be determined from the CT image based on the mean CT number of the nodule. Measuring the CT number of a single pulmonary nodule is therefore common practice, and it is an important part of the diagnostic work-up. CT scanners measure bone density with good accuracy, and when phantoms are placed in the field along with the patient, quantitative CT techniques can be used to estimate bone density, which is useful in assessing fracture risk. CT is also quantitative in terms of linear dimensions, and therefore it can be used to accurately assess tumor volume or lesion diameter.

3.1.5 Geometry and Historical Development [10]

3.1.5.1 First Generation: Rotate/Translate, Pencil Beam

CT scanners represent a marriage of diverse technologies, including computer hardware, motor control systems, x-ray detectors, sophisticated reconstruction algorithms, and x-ray tube/generator systems. The first generation of CT scanners employed a rotate/translate, pencil beam system. Only two x-ray detectors were used, and they measured the transmission of x-rays through the patient for two different slices. The acquisition of the numerous projections and the multiple rays per projection required that the single detector for each CT slice be physically moved throughout all the necessary positions. This system used parallel ray geometry. Starting at a particular angle, the x-ray tube and detector system translated linearly across the field of view (FOV), acquiring 160 parallel rays across a 24 cm FOV. When the x-ray tube/detector system completed its translation, the whole system was rotated slightly, and then another translation was used to acquire the 160 rays in the next projection. This procedure was repeated until 180 projections were acquired at 1-degree intervals.

3.1.5.2 Second Generation: Rotate/Translate, Narrow Fan Beam

The next incremental improvement to the CT scanner was the incorporation of a linear array of 30 detectors. This increased the utilization of the x-ray beam by 30 times, compared with the detector used per slice in first-generation systems. A relatively narrow fan angle of 10 degree was used. In principle, a reduction in scan time of about 30-fold could be expected. However, this reduction time was not realized, because more data were acquired to improve image quality.

3.1.5.3 Third Generation: Rotate/Rotate, Wide Fan Beam

The number of detectors used in the third-generation scanners was increased substantially (to more than 800 detectors), and the angle of the fan beam was increased so that the detector array formed an arc wide enough to allow the x-ray beam to interrogate the entire patient. Because detectors and the associated electronics arc expensive, this led to more expensive CT scanners. However, spanning the dimensions of the patient with an entire row of detectors eliminated the need for translation motion. The multiple detectors in the detector array capture the same number of ray measurements in one instant as was required by a complete translation in the earlier scanner systems. The mechanically joined x-ray tube and detector array rotation together around the patient without translation. The motion of third-generation CT is rotate/translate, referring to the rotation of the x-ray tube and the rotation of the detector array. By elimination of the translational motion, the scan time is reduced substantially.

3.1.5.4 Fourth Generation: Rotate/Stationary

Fourth-generation CT scanners were designed to overcome the problem of ring artifacts. With fourth-generation scanners, the detectors are removed from the rotating gantry and are placed in a stationary 360-degree ring around the patient, requiring many more detectors. Modern fourth-generation CT systems use about 4,800 individual detectors. Because the x-ray tube rotates and the detectors are stationary, fourth-generation CT is said to use a rotate/stationary geometry. During acquisition with a fourth-generation scanner, the divergent x-ray beam emerging from the x-ray tube forms a fan-shaped x-ray beam. However, the data are processed for fan beam reconstruction with each detector as the vertex of a fan, the rays acquired by each detector being fanned out to different positions of the x-ray source.

3.1.5.5 Fifth Generation: Stationary/Stationary

A novel CT scanner has been developed specifically for cardiac tomographic imaging. This cine-CT scanner does not use a conventional x-ray tube; instead, a large arc of tungsten encircles the patient and lies directly opposite to the detector ring. X-rays arc produced from the focal track as a high-energy electron beam strikes the tungsten. There are no moving parts to this scanner gantry. The electron beam is produced in a cone-like structure (a vacuum enclosure) behind the gantry and is electronically steered around the patient so that it strikes the annular tungsten target. Cine-CT systems, also called electron beam scanners, are marketed primarily to cardiologists. They are capable of 50-msec scan times and can produce fast-frame-rate CT movies of the beating heart.

3.1.5.6 Sixth Generation: Helical

In the early 1990s, the design of third- and fourth-generation scanners evolved to incorporate slip ring technology. A slip ring is a circular contract with sliding brushes that allows the gantry to rotate continually, untethered by wires. The use of slip-ring technology eliminated the inertial limitations at the end of each slice acquisition, and the rotating gantry was free to rotate continuously throughout the entire patient examination. This design made it possible to achieve greater rotational velocities than with systems not using a slip ring, allowing shorter scan times. Helical CT (also inaccurately called spiral CT) scanners acquire data while the table is moving; as a result, the x-ray source moves in a helical pattern around the patient being scanned. Helical CT scanners use either third- and fourth-generation slip-ring designs. By avoiding the time required to translate the patient table, the total scan time required to image the patient can be much shorter. Consequently, helical scanning allows the use of less contrast agent and increase patient throughput. In some instances the entire scan can be performed within a single breath-hold of the patient, avoiding inconsistent levels of inspiration. The advent of helical scanning has introduced many different considerations for data acquisition. In order to produce reconstructions of planar sections of the patient, the raw data from the helical data set are interpolated to approximate the acquisition of planar reconstruction data. The speed of the table motion relative to the rotation of the CT gantry is a very important consideration, and the pitch is a parameter that describes this relationship.

3.1.5.7 Seventh Generation: Multiple Detector Array

X-ray tubes designed for CT have impressive heat storage and cooling capabilities, although the instantaneous production of x-rays (i.e., x-rays per milliampere-second [mAs]) is constrained by the physics governing x-ray production. An approach to overcoming x-ray tube out put limitations is to makes better use of the x-rays that are produced by the x-ray tube. When multiple detector array are used, the collimator spacing is wider and therefore more of the x-ray that are produced by the x-ray tube are used in producing image data. With conventional, single detector array scanners, opening up the collimator increases the slice thickness, which is good for improving the utilization of the x-ray beam but reduce spatial resolution in the slice thickness dimension. With the introduction of multiple detector arrays, the slice thickness is determined by the detector size and not by the collimator.

3.1.6 CT-simulation Process [3]

A CT-simulation consists of a CT-scanner with a flat table top, laser patient positioning and marking system (preferably external lasers), CT-simulation/3D treatment planning software, and various hardcopy output devices (Fig. 3.5). The CT-scanner is used to acquire a volumetric CT-scan of a patient, which represents the virtual or geometric digital patient. The CT-simulation software provides virtual representations of the capabilities of a treatment machine. This software can be a special virtual simulation program or it can be a component of a treatment planning system. Often, CT-simulation is referred to as virtual simulation and the two terms tend to be used interchangeably. Virtual simulation is used to define any simulation based on software created virtual simulator and volumetric patient scan. The scandoes not necessarily have to be CT and other imaging modalities can be used. A virtual simulator is set of software which recreates the treatment machine and which allows import, manipulation, display, and storage of images from CT and/or other imaging modalities. The simulation process design is dependent on available resources (equipment and personnel), patient workload, physical layout and location of system components, and proximity of team member. The CT-simulation process can be grouped into three major categories.

3.1.6.1 CT-scan, Patient Positioning and Immobilization

The CT-simulation scan is, in many respects, similar to conventional diagnostic scans. The primary differences are the requirements for patient positioning and immobilization, treatment specific scan protocols, often increased scan limits use of contrast, placement of localization marks on the patient skin, and some other special considerations.

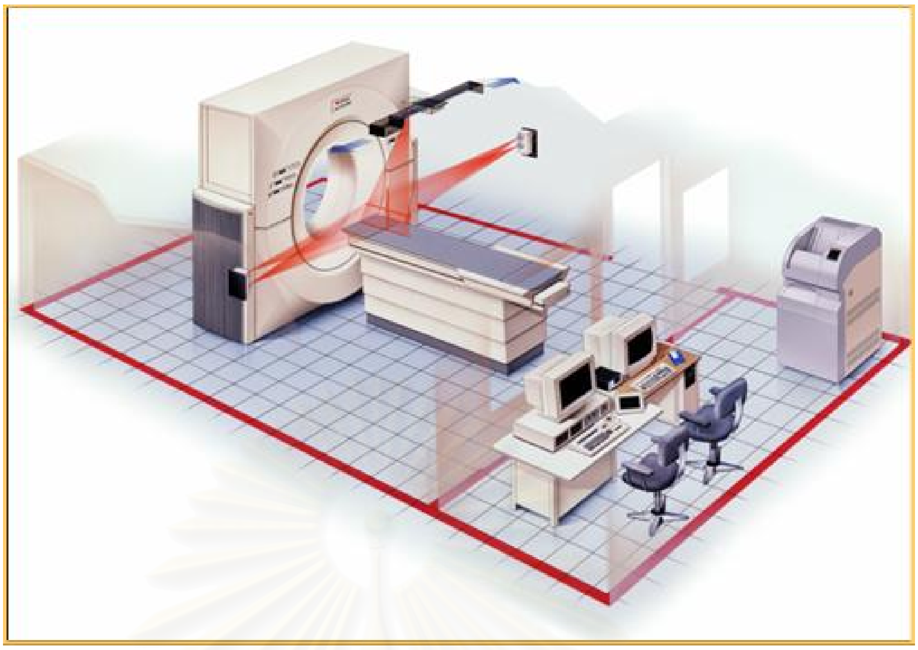

Figure 3.5 The CT-simulation system

3.1.6.2 Treatment Planning and CT-simulation

Beam placement and treatment design is performed using virtual simulation software. This simulation typically consists of contouring of the target and normal structures, placement of the treatment isocenter and the beams, design of treatment portal shapes, generation of DRRs and documentation.

3.1.6.2.1 Contouring

The treatment planning portion of the CT-simulation process begins with target and normal structure delineation. Other imaging studies (prior CT, MR, PET) may be registered (fused) to the CT-scan to provide information for improved target or normal structure delineation.

3.1.6.2.2 Treatment Isocenter Placement

Based on target volumes and treatment area, a treatment isocenter location is identified in the CT study. The isocenter may be placed manually, based on patient anatomy, or the CT-simulation software may automatically position the isocenter at the centroid of the contoured target volume. Once the isocenter is determined or marked, this coordinate becomes part of the treatment plan and may be used as a reference location in subsequent dose calculations. There must be a set of location marks on the patient's skin so that the patient can be accurately repositioned on the treatment machine.

3.1.6.2.3 Placement of the Beams and Design of Treatment Portals

Based on target geometry, treatment beams are placed and treatment portals designed. CT-simulation data (images, contours, treatment beams) are then communicated to treatment planning software, which has dose calculation capabilities.

3.1.6.2.4 Printing of DRRs and Documentation

The final products of the CT-simulation are DRRs and patient setup instructions. Patient setup instructions may include possible shifts from the initial skin localization marks, if final isocenter marking procedures were not used.

3.1.6.3 Treatment Setup

On the treatment machine, the patient is setup according to instructions created from the CT-simulation software. Port films are acquired and compared with CT-simulation DRRs. In some cases, the patient may undergo treatment setup verification on a conventional simulator prior to the treatment.

3.2 Image Quality [10]

Image quality is a generic concept that applies to all types of images. It applies to medical images, photography, television images, and satellite reconnaissance images. Quality is a subjective notion and is dependent on the function of the image. In radiology, the outcome measure of the quality of a radiologic image is its usefulness in determining an accurate diagnosis. It is important to establish at the outset that the concepts of image quality discussed below are fundamentally and intrinsically related to the diagnostic utility of an image. Large masses can be seen on poor-quality images, and no amount of image fidelity will demonstrate pathology that is too small or faint to be detected. The true test of an imaging system, and of the radiologist that uses it, is the reliable detection and accurate depiction of subtle abnormalities. With diagnostic excellence as the goal, maintaining the highest image fidelity is possibly crucial to the practicing radiologist and to his or her imaging facility. While technologists take a quick glance at the images they produce, it is the radiologist who sits down and truly analyzes them. Consequently, understanding the image characteristics that comprise image quality is important so that the radiologist can recognize problems, and articulate their cause, when they do occur.

3.2.1 Noise

Figure 3.6 shows three isometric images; each one has similar contrast, but the amount of noise increases toward the right of the figure. Noise interjects a random or stochastic component into the image (or other measurement), and there are several different sources of noise in an image. There are different concepts pertaining to noise that are useful as background to this topic. Noise adds or subtracts to a measurement value such that the recorded measurement differs from the actual value. Most experimental systems have some amount of noise, and some have a great deal of noise. If we measure some value repeatedly, for instance the number of counts emitted from a weak radioactive source, we can compute the average count rate (decays/second), and there are ways to calculate the standard deviation as well. In this example, multiple measurements are made to try to improve the accuracy of the mean value because there are large fluctuations in each individual measurement. These fluctuations about the mean are stochastic in nature, and the determination of the standard deviation (σ) relates to the precision of the measurement.

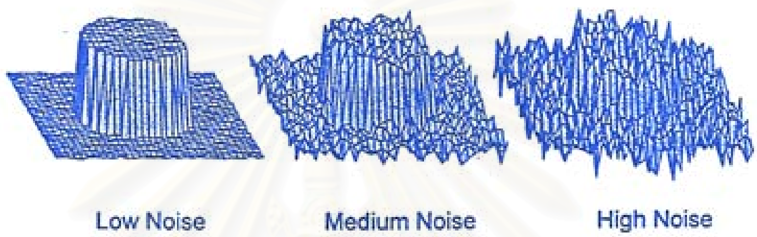

Figure 3.6 Isometric display for the concept of noise

Many types of data have a normal distribution. The normal distribution is also known as the Gaussian distribution, and its mathematical expression is

$$G(x) = ke^{-\frac{1}{2}\left(\frac{\bar{x}-x}{\sigma}\right)^2} \qquad [3.4]$$

Notice that these two parameters, $\overline{X}$ and σ, describe the shape of the Gaussian distribution. The parameter x in Equation 3.4 is called the dependent variable, the value of k is just a constant, used to normalize the height of the curve.

3.2.2 Contrast

Contrast is the difference in the image gray scale between closely adjacent regions on the image. The human eye craves contrast; it is the pizzazz in the image. The very terms that describe low contrast images, such as flat or washed out, have negative connotations. The contrast present in a medical image is the result of a number of different steps that occur during image acquisition, processing, and display. The contrast depends on mAs, dose, pixel size, slice thickness, reconstruction filter, patient size, and gantry rotation speed.

The ability to detect a low-contrast object on an image is highly related to how much noise (quantum noise and otherwise) there is in the image. As noise levels decrease, the contrast of the objects is the essence of contrast resolution. Better contrast resolution implies that more subtle objects can be routinely seen on the image. Contrast resolution is very much related to the SNR. A scientist working on early television systems, Albert Rose, showed that to reliable identify an object, the SNR needed to be better than about 5. This requirement has become known as Rose's criterion. It is possible to identify objects with SNRs lower than 5.0; however, the probability of detection is lower than 100%.

3.2.3 Spatial Resolution [10, 11]

Spatial Resolution is defined as the ability to distinguish two objects placed close together in a noiseless field [11]. The Spatial resolution depends on detector pitch, detector aperture, number of views, number of rays, focal spot size, object magnification, slice thickness, slice sensitivity profile, helical pitch, reconstruction kernel, pixel matrix, patient motion, and field of view [10].

A two-dimensional image really has three dimensions: height, width, and gray scale. The height and width dimensions are spatial (usually), and have units such as millimeters. Spatial resolution is a property that describes the ability of an imaging system to accurately depict objects in the two spatial dimensions of the image. Spatial resolution is sometimes referred to simply as the resolution. The classic notion of spatial resolution is the ability of an image system to distinctly depict two objects as they become smaller and closer together. The closer together they are, with the image still showing them as separate objects, the better the spatial resolution. At some point, the two objects become so close that they appear as one, and at this point spatial resolution is lost.

Compared with x-ray radiography, CT has significantly worse spatial resolution and significantly better contrast resolution. The MTF, the fundamental measurement of spatial resolution, was shown in Fig. 3.7 for a typical CT scanner; it should be compared with the typical MTF for radiography. Whereas the limiting spatial frequency for screen-film radiography is about 7 line pairs (lp) per millimeter and for digital radiography it is 5 lp/mm, the limiting spatial frequency for CT is approximately 1 lp/mm.

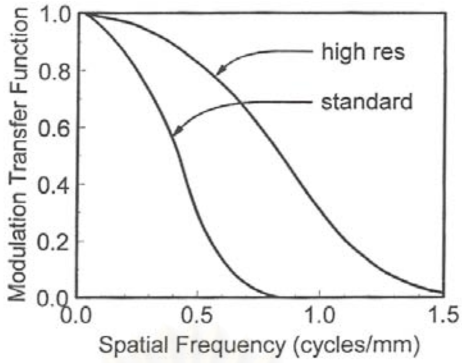

Figure 3.7 The modulation transfer function (MTF) for standard and high-resolution clinical computed tomographic scanners

It is the contrast resolution of CT that distinguishes the modality: CT has, by refers so the ability of an imaging procedure to reliably depict very subtle differences in contrast. It is generally accepted that the contrast resolution of screen-film radiography is approximately 5% whereas CT demonstrates contrast resolution of about 0.5%. A classic clinical example in which the contrast resolution capability of CT excels is distinguishing subtle soft tissue tumors: The difference in CT number between the tumor and the surrounding maybe small (e.g., 20 CT numbers), but because the noise in CT numbers is smaller (e.g., 3 CT numbers), the tumor is visible on the display to the trained human observer. As is apparent from this example, contrast resolution is fundamentally tied to the SNR. The SNR is also very much related to the number of x-ray quanta used per pixel in the image. If one attempt to reduce the pixel size (and thereby increase spatial resolution) and the dose levels are kept the same, the number of x-rays per pixel is reduced. For example, for the same FOV and dose, changing to a 1024×1024 CT image from a 512×512 image would result in fewer x-ray photons passing through each voxel, and therefore the SNR per pixel would drop. It should be clear from this example that there is a compromise between spatial resolution and contrast resolution. In CT there is a well-established relationship among SNR, pixel dimensions (Δ), slice thickness (T), and radiation dose (D):

$$D \propto \frac{SNR^2}{\Delta^3 T} \qquad [3.5]$$

The clinical utility of any modality lies in its spatial and contrast resolution.

3.2.4 The Modulation Transfer Function (MTF(f))

Let's start with a series of sine waves of different spatial frequencies, as shown in Fig. 3.7. The six sine waves shown in Fig. 3.8 have spatial frequencies of 0.5, 1.0, 1.5, 2.0, 2.5, and 3.0 cycles/mm, and these correspond to object sizes of 1.0, 0.50, 0.333, 0.25, 0.40, and 0.167 mm, respectively. Each sine wave serves as an input to a hypothetical imaging system, and the amplitude of each input sine waves corresponds to 100 units. The amplitude here is a measure of the image density (e.g., optical density for film, or gray scale units for a digital image) between the peak and valleys of the sine wave. Each of the input sine waves is blurred by the point spread function of the imaging system, and the resulting blurred response to each sine wave (the output of the imaging system) is shown in Fig.3.8 as dotted lines. Notice that as the spatial frequency increases, the blurring causes a greater reduction in the output amplitude of the sine wave.

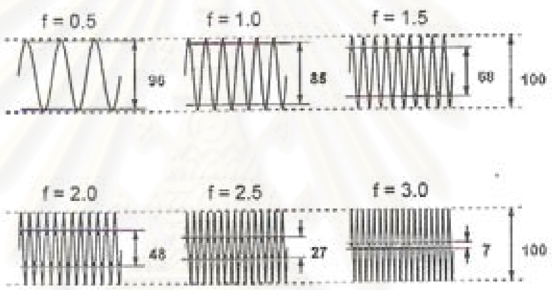

Figure 3.8 A series of sine waves of differing spatial frequencies

The amplitude of the sine wave is really just the contrast between the peaks and valleys. All six sine waves in Fig.3.8 have the same input contrast to the hypothetical imaging system (100 units), but the output contrast was altered by the blurring influence of the point spread function. The output contrast is lower for higher spatial frequencies (i.e., smaller objects), and is identified on Fig.3.8 by two horizontal lines for each sine wave. The modulation is essentially the output contrast normalized by the input contrast. The modulation transfer function (MTF) of an imaging system is a plot of the imaging system's modulation versus spatial frequency. In Fig.3.9, the output modulation for each of the sine waves shown in Fig.3.8 is plotted on the y-axis, and the frequency of the corresponding sine wave is the x-axis value.

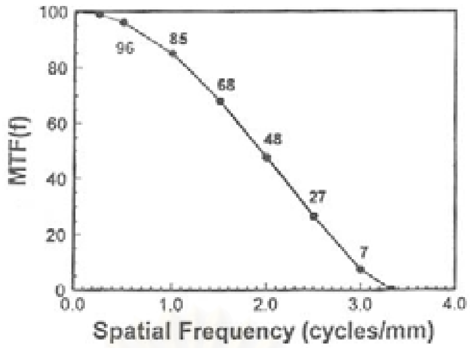

Figure 3.9 The output amplitude of the sine waves illustrated in Fig.3.8

The MTF of an image system, like that shown in Fig.3.9, is a very complete description of the resolution properties of an imaging system. The MTF illustrates the fraction (or percentage) of an object's contrast that is recorded by the imaging system, as a function of the size (i.e., spatial frequency) of the object. To the reader previously unfamiliar with the concept of the MTF, it is fair to ask why imaging scientists prefer to use the MTF to discuss the spatial resolution of an imaging system, over the easier –to-understand spread function description discussed previously. A partial answer is seen in Fig. 3.10. Many imaging systems are really imaging chains, where the image passes through many different intermediate steps from the input to the output of the system (fluoroscopy systems are a good example). To understand the role of each component in the imaging chain, the MTF is measured separately for each component (MTF curves A, B, and C in Fig. 3.10). The total system MTF at any frequency is the product of all the subcomponent MTF curves.

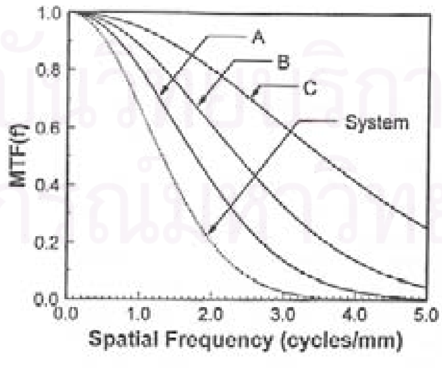

Figure 3.10 An imaging system is often made of a series of components, and the MTFs for components A, B, and C

3.3 **Radiation Dose in Computed Tomography** [12]

Because of its geometry and usage, CT is a unique modality and therefore has its own set of specific parameters for radiation dose. This modality is unique because the exposure is essentially continuous around the patient, rather than a projectional modality in which the exposure is taken from one or two source locations. The modality typically uses thin sections ranging from 0.5 mm to 20 mm nominal beam collimation. However, this modality also typically uses multiple exposures along some length of the patient to cover a volume of anatomy. In addition, these exposures may be done in sequences of scans (e.g., a series of scans such as pre- and post-contrast).

3.3.1 Variations within the Scan Plane

Projectional radiographic exposures are taken from one source position and the entrance skin dose is much larger than the exit dose, creating a large radiation dose gradient across the patient. In contrast, the tomographic exposure of CT scans with a full 360° rotation results in a radially symmetric radiation dose gradient within patient. That is, in a uniform circular object, such as a test phantom, all of the points at a certain radius from the center have the same (or nearly the same) radiation dose. As we shall see, the magnitude of that dose gradient (the size of the difference from center to periphery) will be affected by several factors, including the size of the object, the x-ray beam spectrum, and the attenuation of the material or tissue.

For example, in a typical CT dosimetry phantom that is 32 cm in diameter and made of polymethyl methacrylate (PMMA) usually referred to as the body phantom measurements of CT dose, which will be defined later, obtained at the center are typically about 50% of the measured value obtained at one of the peripheral positions. This result which shows the center value obtained under specific conditions to be approximately 10 mGy while the peripheral values are 20 mGy under those same conditions. However, for a smaller-diameter phantom the 16 cm diameter phantom referred to as the head phantom measured under the identical exposure conditions, the center value reading climbs to approximately 40 mGy, as do the peripheral values. This indicates that the magnitude of the difference from center to periphery is very much size dependent; it also indicates that the absolute values of the absorbed doses are size dependent.

3.3.2 Z-axis Variations

In addition to variations within the scan plane, there are variations along the length of the patient or phantom. These can be characterized by the z-axis dose distribution or radiation profile. This is the distribution of absorbed dose along the axis of the patient due to a single axial scan (a full rotation at one table position). The radiation profile is not limited to the primary area being imaged, and there are tails to this distribution from the nonideal collimation of the x-ray source and from scatter of photons within the object being exposed. When multiple adjacent scans are performed, the tails of the radiation profiles from adjacent scans can contribute to the absorbed dose outside of the primary area being imaged. If these tails are significant and are nonzero at some distance from the location of the originating section, then those contributions can add up, creating additional absorbed dose in the primary are being imaged.

That is the radiation dose in a specific section consist of the sum of contributions to that section when that area is the primary area being imaged as well as the contributions from the tails of radiation profiles from adjacent sections when other locations are the primary are being imaged. The size of the contributions from adjacent sections is very directly related to the spacing of sections and the width and shape of the radiation profile.

To account for the effects from multiple scans, several dose descriptors were developed. One of the first was the multiple scan average dose (*MSAD*) descriptors. This is defined as the average dose resulting from a series of scans over n interval (I) in length:

$$MSAD = \left(\frac{1}{I}\right)\int_{-I/2}^{I/2} D_{series}\left(z\right)dz \qquad [3.6]$$

where I is the interval of the scan length and $D_{series}(z)$ is the dose at position z parallel to the z (rotational) axis resulting from the series of CT scans.

Following this was the computed tomography dose index (*CTDI*). This was defined as the radiation dose, normalized to beam width, measured from 14 contiguous sections:

$$CTDI = \left(\frac{1}{nT}\right)\int_{-7T}^{7T} D_{single}\left(z\right)dz \qquad [3.7]$$

where n is the number of sections per scan, T is the width of the interval equal to the selected section thickness, and $D_{single}(z)$ is the dose at the point z on any line parallel to the z (rotational) axis for a single axial scan. This index was suggested by the Food and Drug Administration and incorporated into the Code of Federal Regulation.

However, to be measured according to the definition, only 14 sections could be measured and one had to measure the radiation dose profile typically done with thermoluminescent dosimeters (TLDs) or film, neither of which was very convenient. Measurements of exposure could be obtained with a pencil ionization chamber, but its fixed length of 100 mm meant that 14 sections of 7 mm thickness could be measured with the chamber alone. To measure CTDI for thinner nominal sections, sometimes lead sleeves were used to cover the part of the chamber that exceeded 14 section widths.

To overcome the limitations of CTDI with 14 sections, another radiation dose index $CTDI_{100}$ was developed. This index relaxed the constraint on 14 sections and allowed calculation of the index for 100 mm along the length of an entire pencil ionization chamber, regardless of the nominal section width being used. This index is therefore defined as

$$CTDI_{100} = \left(\frac{1}{NT}\right)\int_{-5cm}^{5cm} D_{single}(z)\,dz \qquad [3.8]$$

where N is the number of acquired sections per scan (also referred to as the number of data channels used during acquisition) and T is the nominal width of each acquired section (which is not necessarily the same as the nominal width of the reconstructed section width).

Because the ionization chamber measures an integrated exposure along its 100 mm length, this is equivalent to

$$CTDI_{100} = (f \cdot C \cdot E \cdot L)/(NT) \qquad [3.9]$$

where f is the conversion factor from exposure to a dose in air (use 0.87 rad/R), C is the calibration factor for the electrometer, E is the measured value of exposure in roentgens acquired from a single 360° rotation with a beam profile of NT (as defined earlier), L is the active length of the pencil ionization chamber, and N and T are as defined for equation 3.8.

Thus, the exposure measurement, performed with one axial scan either in air or in one of the polymethy methacrylate phantoms for which CTDI is defined, result in a calculated for the center location as well as at least one of the peripheral position (1 cm below the surface) within the phantom to describe the variations within the scan plane as well.

$CTDI_w$ was created to represent a dose index that provides a weighted average of the center and peripheral contributions to dose within the scan plane. The index is used to overcome the limitations of $CTDI_{100}$ and its dependency on position within the scan plane. The definition is

$$CTDI_w = \left(\frac{1}{3}\right)\left(CTDI_{100}\right)_{center} + \left(\frac{2}{3}\right)\left(CTDI_{100}\right)_{periphery} \qquad [3.10]$$

CHAPTER IV

RESEARCH QUESTION AND RESEARCH OBJECTIVE

4.1 Research Questions

4.1.1 Primary Question

How the physical performance and radiation dose of the recently therapeutic multi-slice CT simulator scanner are difference from the diagnostic multi-slice CT scanner, produced from the same manufacturer?

4.1.2 Secondary Question

Is the manufacturer supply phantom reliable to be used for routine test?

4.2 Research Objectives

4.2.1 To study the physical performance from the therapeutic multi-slice CT scanner and compare with the diagnostic multi-slice CT scanner for the same parameter setting

4.2.2 To find the radiation dose of the therapeutic multi-slice CT scanner and compare with the diagnostic multi-slice CT scanner for the same parameter setting

4.2.3 To test a reliable of manufacturer supply phantom by compare with the independent phantom (CATPHAN).

CHAPTER V

RESEARCH METHODOLGY

5.1 Research Design

This study is a descriptive observational cross sectional study design.

5.2 Research Design Model

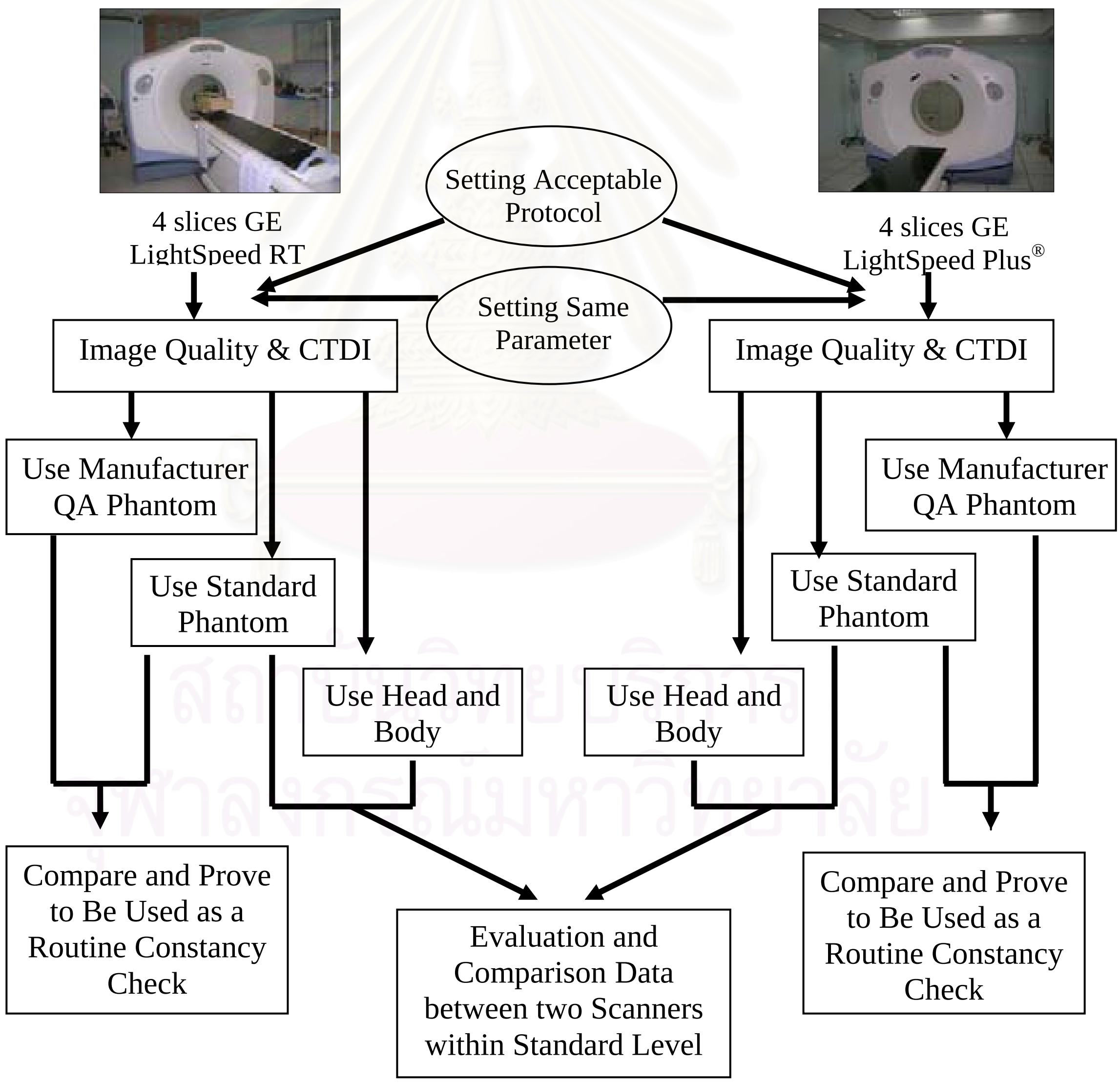

5.3 Conceptual Framework

Parameters : kVp, Slice width, Number of slice, Mode, FOV, Length of scanning, mA, pitch, Algorithm, Feed/Rotation, Rotation time

↓

Isocenter to Tube Distance, Tube Focus to Detector Distance

↓

Physical performance
(Image quality & Radiation Dose)

↓

- Slice thickness accuracy
- CT number accuracy and linearity
- Image uniformity
- Image noise
- Low-contrast resolution
- High-contrast resolution
- CTDI

5.4 Key Word

- Multi-slice CT
- CT radiation exposure
- CT image quality
- CT simulator

5.5 Material

5.5.1 The Diagnostic CT Scanner [5]

The diagnostic CT scanner (GE LightSpeed Plus®) which is shown in Fig. 5.1 is a premium-tier, 7^{th} generation CT scanner (The x-ray tube rotates and the detectors rotate, wide fan beam). It is the ability to simultaneously collect 4 rows of scan data. This 4-row data collection is accomplished via a 16-row detector and a 4-row DAS. The distance from tube focus spot to imaging isocenter is 541 mm. The distance from tube focus spot to detector is 949 mm. Remote tilt gantry from operator console is ±30º. The maximum SFOV is 500 mm. Bore diameter is 700 mm. An x-ray tube has a Tungsten-Rhenium focal track on a molybdenum alloy substrate back by graphite target with maximum heat capacity of 6.3 MHU. Four kVp settings are available (80, 100, 120 and 140 kVp). Exposure techniques range from 10 to 400 mA in 10-mA increments with five scan time setting (0.8, 1, 2, 3, 4s) and seven reconstruction algorithms (soft, standard, lung, detail, bone, edge and bone plus).

Figure 5.1 The diagnostic CT scanner (GE LightSpeed Plus®)

5.5.2 The Therapeutic CT Simulator Scanner [4]

The therapeutic CT simulator scanner (GE LightSpeed RT) which is shown in Fig.5.2 is a premium-tier, 7^{th} generation CT scanner (The x-ray tube rotates and the detectors rotate, wide fan beam) with external dimensions similar to those of the LightSpeed Plus CT scanner. It is the ability to simultaneously collect 4 rows of scan data. This 4-row data collection is accomplished via a 16-row detector and a 4-row DAS. The distance from tube focal spot to imaging isocenter is 606 mm. The distance from tube focus spot to detector is 1062 mm. Remote tilt gantry from operator console is ±30º. The maximum SFOV is 650 mm. Bore diameter is 800 mm. An x-ray tube has a Tungsten-Rhenium focal track on a molybdenum alloy substrate back by graphite target with maximum heat capacity of 7.5 MHU. Four kVp settings are available (80, 100, 120 and 140 kVp). Exposure techniques range from 10 to 400 mA in 5-mA increments with four scan time setting (1, 2, 3, 4s) and seven reconstruction algorithms (soft, standard, lung, detail, bone, edge and bone plus).

Figure 5.2 The therapeutic CT simulator scanner (GE LightSpeed RT)

The major differences between the two systems are shown in Table 5.1.

Table5.1 The difference characteristics of GE LightSpeed Plus® and LightSpeed RT

Characteristics	**GE LightSpeed Plus®**	**GE LightSpeed RT**
Gantry bore	70 cm.	80 cm.
Isocenter to tube distance	54 cm.	60.6 cm.
Tube focus to detector distance	95 cm.	106.25 cm.
Max. SFOV	50 cm.	65 cm.
Scan time setting	0.8, 1, 2, 3 and 4	1, 2, 3 and 4
Couch structure	Curve	Flat
Moving Laser	Not available	Available
Virtual simulation	Not available	Available
Heat capacity	6.3 MHU	7.5 MHU

5.5.3 CATPHAN Phantom [13]

Fig. 5.3 shows the CATPHAN phantom (The Phantom Laboratory, New York, NY) which contains four modules. The phantom can assess both mechanical integrity and image quality of a CT scanner. It has a modular design, and within each module, different image quality parameters can be evaluated. Each module is illustrated in Fig. 5.4

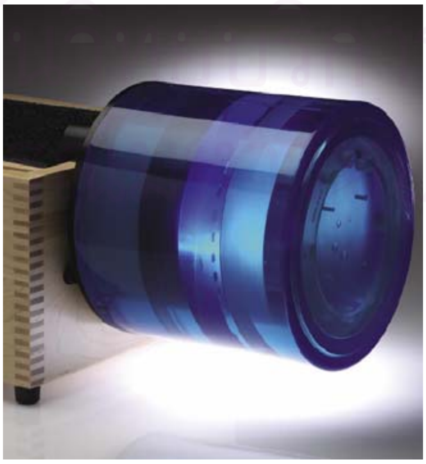

Figure 5.3 CATPHAN phantom

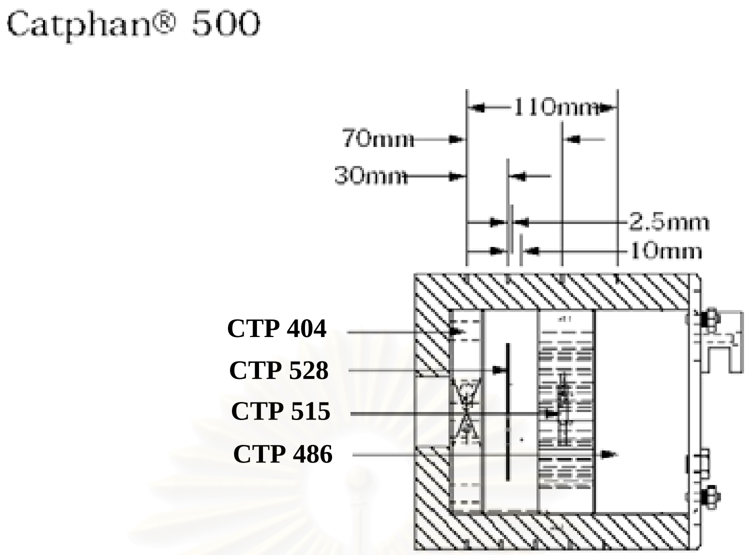

Figure 5.4 Illustration of test module location of Catphan® 500 phantom

The CATPHAN phantom is designed so all test sections can be located by precisely indexing the table from the center of section 1 (CTP404) to the center of each subsequent test module. This design eliminates the need to remount the phantom once the position of section 1 (CTP404) has been verified. The indexing distances from section 1 are listed below.

CATPHAN test module locations:

Module	Distance from section 1 center
CTP404, slice width, sensitometry and pixel size	reference
CTP528, 21 line pair high resolution	30mm
CTP528, Point source	40mm
CTP515, Sub-slice and supra-slice low contrast	70mm
CTP486, Solid image uniformity module	110mm

5.5.3.1 CTP404: Module with Slice Width, Sensitometry (CT number linearity) and Pixel Size

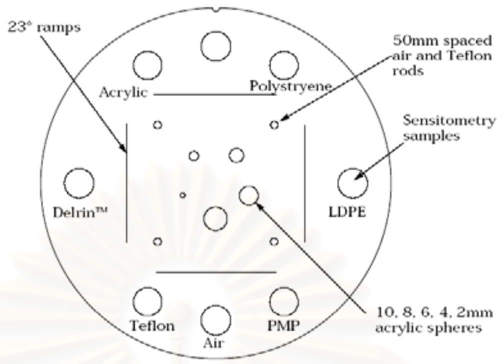

Figure 5.5 CTP404: 1st part of Catphan® 500 phantom

Module 404 which is shown in Fig.5.5 contains seven inserts (acrylic, air, polystyrene, LDPE, PMP, Teflon, and Delrin™). They are used to characterize the accuracy and linearity of CT numbers. This Module has two pairs of 23º wire ramps that are used to estimate slice width measurements.

5.5.3.2 CTP528: High Resolution Module with 21 Line Pair per cm Gauge and Point Source

Figure 5.6 CTP528 : 2nd part of Catphan® 500 phantom

This section has a 1 through 21 line pair per centimeter high resolution test gauge and two impulse sources (beads) which are cast into a uniform material. The beads are positioned along the y axis 20mm above or below the phantom’s center and

2.5 and 10mm past the center of the gauge in the z direction. On older CTP528 modules, the bead is aligned in the z axis with the gauge.

5.5.3.3 CTP515: Low Contrast Module with Supra-slice and Subslice Contrast Targets

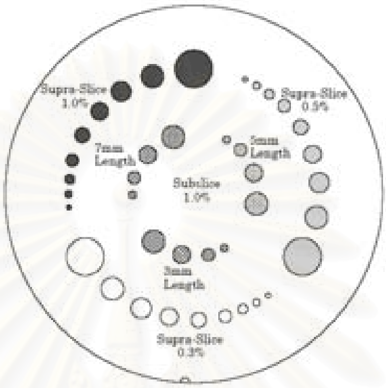

Figure 5.7 CTP515 : 3rd part of Catphan® 500 phantom

The low contrast targets which are shown in Fig.5.7, they have the following diameters and contrasts: Supra-slice target diameters are 2.0mm, 3.0mm, 4.0mm, 5.0mm, 6.0mm, 7.0mm, 8.0mm, 9.0mm, and 15.0mm with nominal target contrast 0.3%, 0.5% and 1.0% levels, Subslice target diameters are 3.0mm, 5.0mm, 7.0mm, and 9.0mm with only nominal target contrast 1.0% level..

All of the targets in each contrast group are cast from a single mix to assure that the contrast levels will be the same for all targets.

The equation 5.1 can be used to convert the measured contrasts and diameters to other specified contrasts and diameters.

$$\text{(Measured Contrast)} \times \text{(smallest diameter discernible)} \cong \text{Constant} \qquad [5.1]$$

Example: 5mm diameter @ 0.3% $\cong$ 3mm diameter @ 0.5%

Along with the supra-slice (targets with z axis dimension longer than most maximum slice width) the CTP515 low contrast module includes subslice targets (targets with z axis length smaller than some of the usual slice width). The subslice targets are arranged in the inner circle of tests in the module.

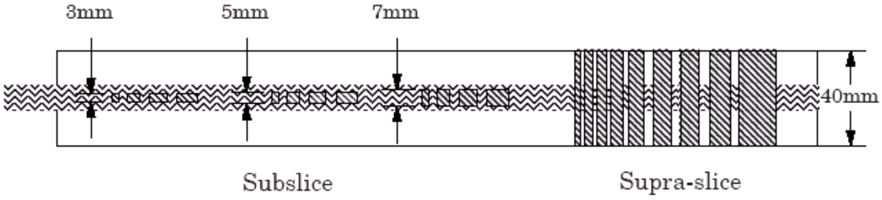

Figure 5.8 Subslice and supra-slice on top view

The subslice targets are cast from the same mix as the 1.0% supra-slice targets. Because they are from the same mix in the evaluation of the actual subslice target contrast the supra-slice targets can be used to establish contrast values. The subslice targets have z axis lengths of 3, 5, and 7mm and diameters of 3, 5, 7, and 9mm. The definition of supra-slice and subslice are shown in Fig. 5.8.

5.5.3.4 CTP486: Image Uniformity Module

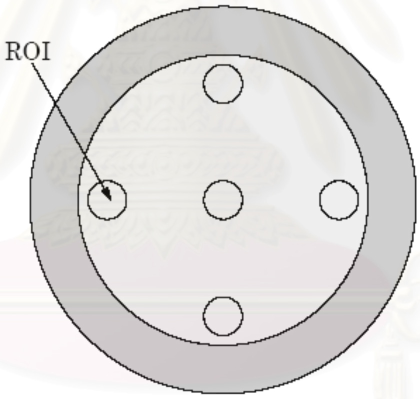

Figure 5.9 CTP486 : 4th part of Catphan® 500 phantom

The image uniformity module is shown in Fig.5.9, it is cast from a uniform material. The material's CT number is designed to be within 2% (20 HU) of water's density at standard scanning protocols. The typically recorded CT numbers range from 5 HU to 18 HU. This module is used for measurements of spatial uniformity, mean CT number and noise value.

5.5.4 Manufacturer QA Phantom [4, 5]

The Quality Assurance Phantom to assess system performance and establish an ongoing Quality Assurance program was used.

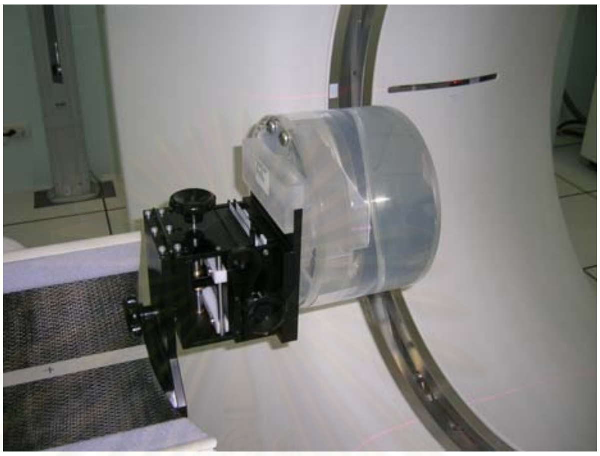

Figure 5.10 Manufacturer QA phantom

The phantom design provides maximum performance information with minimum effort, the phantom equipped on the couch is shown in Fig. 5.10. This phantom could be measured for six aspects of image quality.

- Contrast Scale
- High Contrast Spatial Resolution
- Low Contrast Detectability
- Noise and Uniformity
- Slice Thickness
- Laser Light Accuracy

The QA phantom contains three sections; each corresponding to a single scan plane, the detail of each section is shown in Fig. 5.11.

5.5.4.1 Section 1: Resolution Block

The resolution block which is shown in Fig. 5.11A is at 0 mm scan location. It contains six sets of bar patterns in a Plexiglas block used to test high contrast spatial resolution. Each set of pattern consists of equally sized bars and spaces. Water fills the spaces and provides about 12% (120 HU) contrast. The resolution block contains the following bar sizes: 1.6 mm, 1.3 mm, 1.0 mm, 0.8 mm, 0.6 mm, and 0.5 mm. Both sides of the resolution block contain a pattern of air filled holes designed to demonstrate slice thickness. The resolution block contains holes drilled 1 mm apart and positioned to form a line at 45 degrees to the scan plane. Each visible hole in the image represents 1 mm of beam thickness.

5.5.4.2 Section 2: Contrast Membrane

The location of this section is 40mm superior from the section 1, it is shown in Fig. 5.11B. It contains a doped polystyrene membrane suspended in water and pierced by a series of holes in the following sizes: 10.0 mm, 7.5 mm, 5.0 mm, 3.0 mm, and 1.0 mm.

5.5.4.3 Section 3: Water Bath

Section 3 of the phantom is at 60 mm superior from section 1, it is shown in Fig. 5.11C. It provides a uniform image to assess image CT number noise and uniformity.

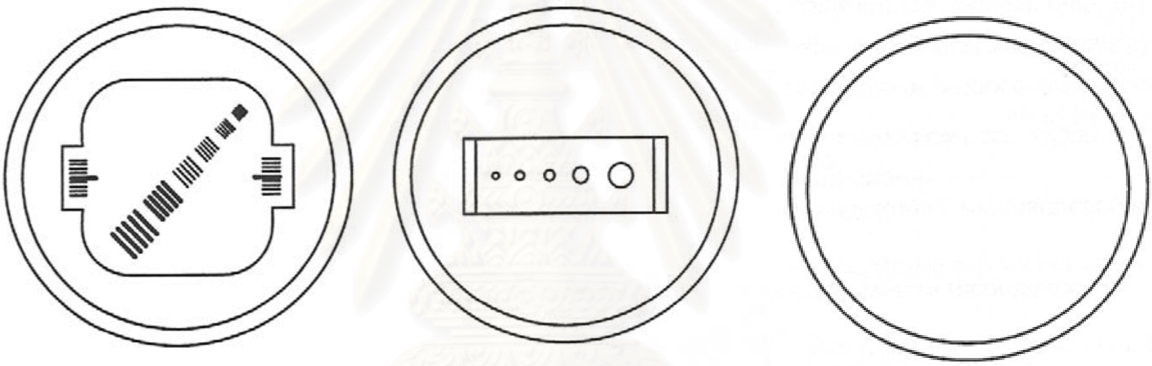

(A) (B) (C)

Figure 5.11 Three sections of QA phantom:
(A) Section 1: Resolution Block
(B) Section 2: Contrast Membrane
(C) Section 3: Water Bath

5.5.5 Ionization Chamber: DCT 10-RS S/N1057 [14]

A 10-cm-long CT pencil ionization chamber is shown in Fig. 5.12. It has 4.9 cm^3 active volume, 100 mm total active length, 8.0 mm inner diameter of out electrode, and 1.0 mm diameter of inner electrode. It is connected with an electrometer.

Figure 5.12 Ionization chamber: DCT 10-RS S/N1057

5.5.6 Electrometer: RTI Electronics AB Type SOLIDOSE 400 Electrometer S/N 4103 [14]

An electrometer which is shown in Fig. 5.13, has the leakage within 4×10^{-15} ampere, 80 – 150 kV radiation quality, and $N_{D,K}$ = 24.2 mGy·cm/nC calibration factor (120 kV/HWD 4.05 mm Al).

Figure 5.13 Electrometer: RTI Electronics AB Type SOLIDOSE 400 Electrometer S/N 4103

5.5.7 Head and Body Phantom

Head phantom which is shown in Fig. 5.14A has 16-cm diameter CTDI polymethylmethacrylate (PMMA) phantom. Body phantom which is shown in Fig. 5.14B has 32-cm diameter CTDI polymethylmethacrylate (PMMA) phantom. The 10-cm-long CT pencil ionization can be placed in the holes of both phantoms. The typical correction-factors in the phantom at 120 kV are shown in Table 5.2.

(A) (B)

Figure 5.14 Cylindrical phantom: (A) Head phantom with 16-cm diameter and (B) Body phantom with 32-cm diameter

Table 5.2 Typical correction-factors in the Phantom at 120 kV [14]

Position	Correction-factor
Central Head	1.04
Peripheral Head	1.06
Central Body	0.99
Peripheral Body	1.06

5.6 **Method**

5.6.1 Display Monitor Checked

In most clinical circumstances, the physician’s interpretation is accomplished from a transparency image recorded with a multiformat camera. Ideally, the transparency image reproduces the quality of the original image displayed on the system monitor, and the display monitor reproduces the available image quality. The following procedure employs the use of the Society of Motion Picture and Television Engineers (SMPTE) digital test pattern [1]. This pattern is available from most CT manufacturers as a stored image data file for setup and assessment of displayed and recorded images.

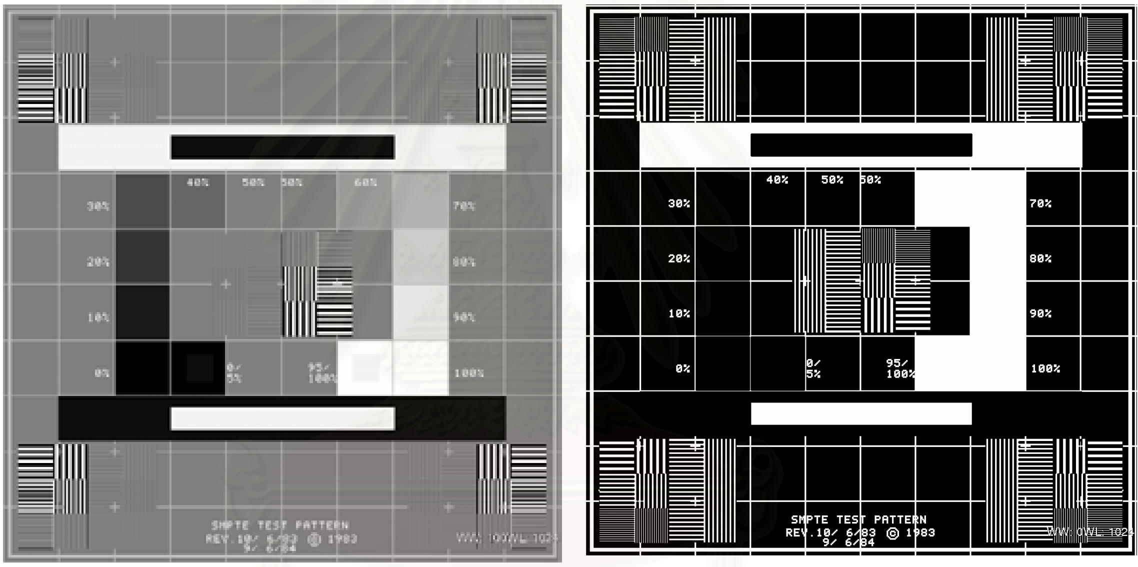

(A) (B)

Figure 5.15 The Society of Motion Picture and Television Engineers (SMPTE) digital test pattern: (A) WW 100 and WL 1024 setting and (B) WW 0 and WL 1024 setting

Display monitor was checked by SMPTE test pattern which is shown in Fig. 5.15 by the following procedure.

Setting	Condition
Window width : 100 Window level : 1024	The 5% patch should just be visible inside of the 0% patch, and the 95% patch should be visible inside the 100% patch (Fig. 5.15 A).
Window width : 0 Window level : 1024	The set of line pattern on the center and the corners have clearly separated lines (Fig. 5.15 B).

5.6.2 Parameter Setting for Image Quality Performance

5.6.2.1 Parameter Setting for CATPHAN Phantom

Equivalent sets of measurements were performed on both the LightSpeed Plus® CT (70-cm bore) and the LightSpeed RT CT (80-cm bore) scanners by using a commercially available CT performance phantom (CATPHAN). The phantom modules are stacked and bolted to a supporting template that has an alignment notch and hanging rods. Exposure techniques used for image quality evaluation (except slice thickness) were set as follows.

Interface	Input
Entry	Head First
Position	Supine
Anatomical Reference	Head
Landmark Location	0 on resolution phantom at circumferential line/cross hatch.
Scan Type	Axial
Slice Thickness	10 mm.
Tilt	0 degrees
SFOV	Small
kV	120
mA	250
Rotation speed	1 sec.
DFOV	25 cm.
Algorithm	Standard
Matrix	512

5.6.2.2 Parameter Setting for Manufacturer Supply Phantom

Both scanners have a Quality Assurance program that tests image quality and geometric integrity of unit by manufacturer supply phantom. Test results were compared with Bench Mark value which was obtained by acceptance test or manufacturer’s criteria. The test should be performed regularly to confirm the performance of the scanner.

The QA test (except slice thickness) was set as follows:

Interface	Input
Entry	Head First
Position	Supine
Anatomical Reference	QA
Landmark Location	0 on resolution phantom at circumferential line/cross hatch.
Scan Type	Helical 0.75:1
Scan Range	I0 – S60
Slice Thickness	10 mm.
Table Speed	15 sec/rot.
Recon Interval	10 mm.
Tilt	0 degrees
SFOV	Small
kV	120
mA	210
Rotation speed	1 sec.
DFOV	25 cm. (phantom diameter: approximately 21.5 cm.)
Algorithm	Standard
Matrix	512

The QA protocol for slice thickness was shown below.

Interface	Input		
Entry	Head First		
Position	Supine		
Anatomical Reference	QA		
Landmark Location	0 on resolution phantom at circumferential line/cross hatch.		
Scan Type	Axial		
Scan Range	Prescribe 4 Groups		
Group	Thickness	Scan Range	Spacing
1	5 mm/ 4i	I7.5 – S7.5	0
2	3.75 mm/ 4i	I5.5 – S5.5	0
3	2.5 mm/ 4i	I3.75 – S3.75	0
4	1.25 mm/ 4i	I1.90 – S1.85	0
Tilt	0 degrees		
SFOV	Small		
kV	120		
mA	330		
Rotation speed	1 sec.		
DFOV	25 cm. (phantom diameter: approximately 21.5 cm.)		
Algorithm	Standard		
Matrix	512		

5.6.3 The Accuracy of Slice Thickness Measurement [1]

The accuracy of slice thickness, which was defined as the full width at half-maximum pixel intensity (or CT number), were measured on manufacturer QA and CATPHAN phantoms.

5.6.3.1 Slice Thickness Measurement by CATPHAN Phantom

Module 404 of the CATPHAN contains two sets of ramp wires angled at 23˚ (Fig. 5.16) that were used to determine scan thickness by determining the length of the wire when the window width is set to 1 and the level is set to the half-maximum CT number of the ramp wire (Fig. 5.17). This window level was determined by first identifying the CT number of the background when the window width was set to 1 and the level was adjusted to a point where the ramp almost disappeared. The CT number of the level at this position is the maximum value. The CT number corresponding to the background was then subtracted from the maximum CT number to establish a range, which was then multiplied by 0.5. This half-range value was added to the background, and the resulting CT number corresponding to the half maximum was determined. The level was then set to this half maximum CT number, and the length of the ramp was measured using the tools provided by the scanner’s software. In order to compensate for the angularity of the ramp in the phantom module, the ramp length measured was then multiplied by tan23º. Four ramp length measurements were used to calculate an average ramp length. Fig. 5.16 shows slice thickness measurement by CATPHAN phantom.

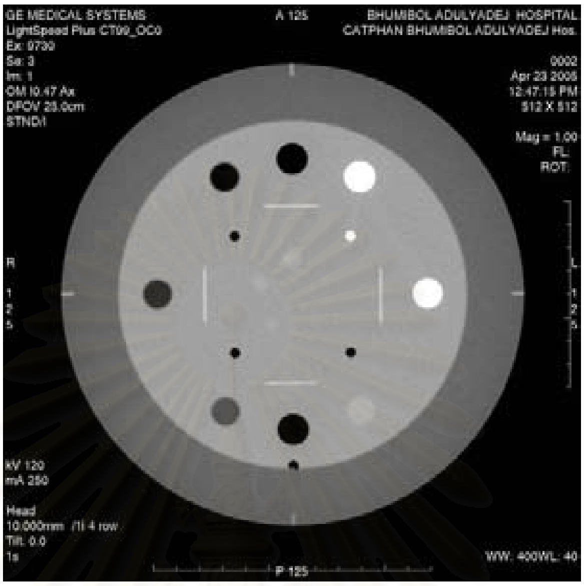

Figure 5.16 Module 404 of CATPHAN phantom

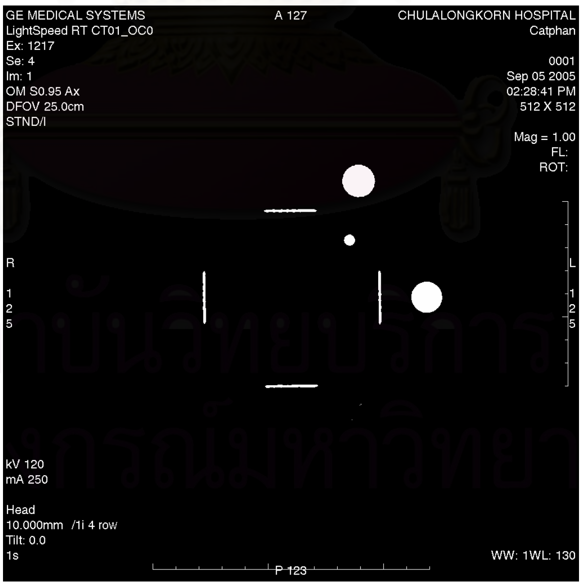

Figure 5.17 Determination of slice thickness by CATPHAN phantom

5.6.3.2 Slice Thickness Measurement by Manufacturer QA Phantom

The manufacturer QA phantom was measured by following the manufacturer's recommended procedures. Section 1 of the phantom was used to determine scan thickness by counting the visible lines when displaying the image (Fig.5.18) at the recommended window width and level (Table 5.3). Each black line represents one millimeter of slice thickness. Gray lines represent fractions of a millimeter. Fig. 5.19 shows the determination of slice thickness measurement by manufacturer QA phantom.

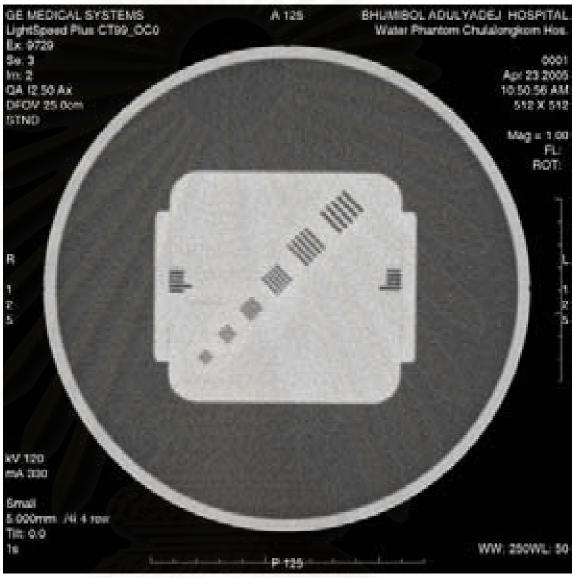

Figure 5.18 Section 1 of manufacturer QA phantom

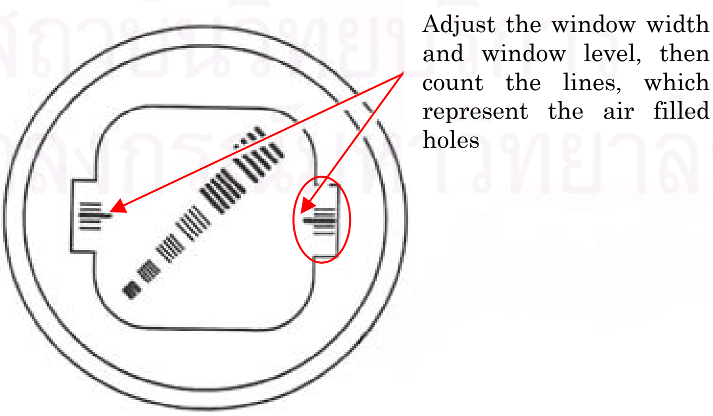

Figure 5.19 Determination of slice thickness

Table 5.3 Recommended window width and level for scan slice thickness measurements [4, 5]

Nominal slice thickness (mm)	Window width	Window level
1.25	100	-100
2.50	100	-25
3.75	100	25
5.00	100	50

5.6.4 CT Number Accuracy and Linearity Measurement

CT number accuracy was characterized using both phantoms. CT number linearity was performed using only CATPHAN phantom.

5.6.4.1 CT Number Accuracy Measurement by CATPHAN Phantom

Module 404 of the CATPHAN (Fig. 5.16) containing seven inserts (Polystyrene, LDPE, PMP, Air, Teflon, Delrin™, and Acrylic) which were used to characterize the accuracy and linearity of CT numbers. CT numbers were measured by circle ROI which were adjusted until the size just located in the insert. The mean reading values were compared with nominal expected values. The nominal expected CT number values [1, 13] were estimated from the linear attenuation coefficients based on a monoenergetic 70-keV photon beam [1]. The graph plotted between linear attenuation coefficient and mean CT number should show linearity then the contrast scale (*CS*) [1, 2] was calculated from this graph. The contrast was defined by

$$CS = \frac{\mu_x - \mu_{water}}{CT_x - CT_{water}} \qquad [5.1]$$

where μ_x = linear attenuation coefficient of material x
μ_{water} = linear attenuation coefficient of water
CT_x = CT number of material x
CT_{water} = CT number of water

This is equivalent to

$$CS = \frac{1}{slope\ of\ the\ CT\ number\ vs.\ linear\ attenuation\ coefficient\ line\ fit} \qquad [5.2]$$

This equation was used in the calculations of *CS* for different CT number data sets [1].

5.6.4.2 CT Number Accuracy Measurement by Manufacturer QA Phantom

Section 3 (Fig. 5.20) of the manufacturer QA phantom was used to characterize CT number accuracy by comparing the mean CT number water in a ROI at the center with the nominal expected value (0 HU).

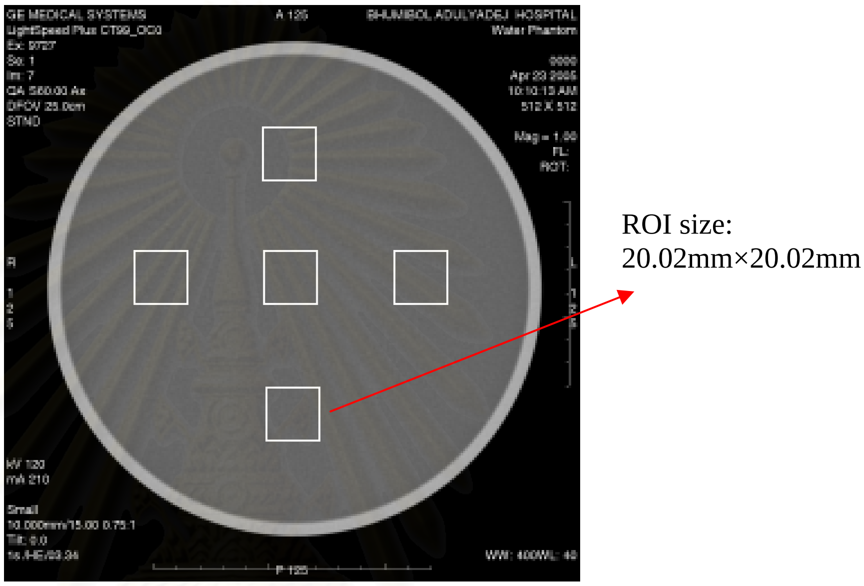

Figure 5.20 Section 3 of manufacturer QA phantom

5.6.5 Image Uniformity Measurement

Image uniformity, measured as the edge-to-center difference in mean CT numbers, was measured using section 3 (Fig. 5.20) of the manufacturer QA phantom and CATPHAN Module 486 (Fig. 5.21). On both phantoms, CT number measurement at the center and four peripheral locations were performed.

5.6.5.1 Image Uniformity Measurement by CATPHAN Phantom

Circular regions of approximately 900 mm^2 were used for CATPHAN measurements. The distance between the center of the ROI at the peripheral locations and the origin is 5 cm. Fig. 5.21 shows uniformity measurement by CATPHAN phantom.

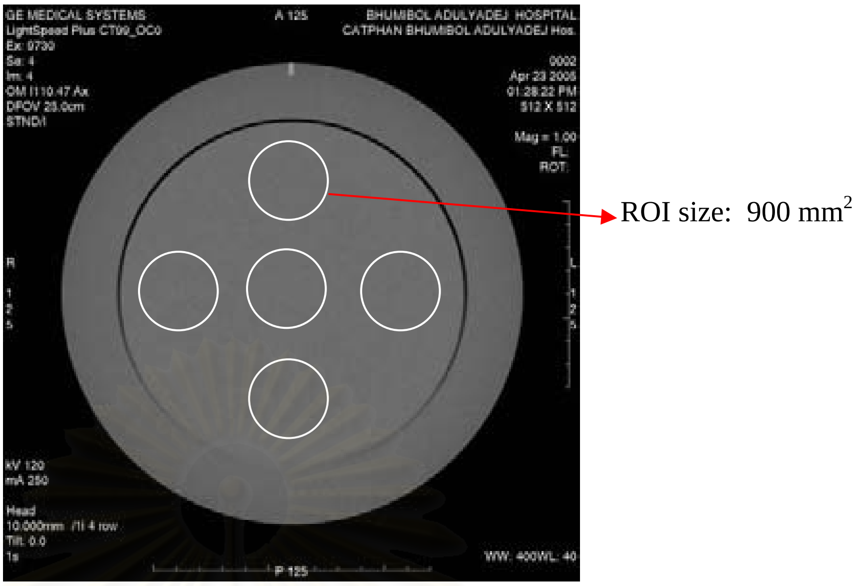

Figure 5.21 Module 486 of CATPHAN phantom

5.6.5.2 Image Uniformity Measurement by Manufacturer QA Phantom

Square regions of approximately 2×2 cm^2 were used for manufacturer QA phantom measurements. The distance between the center of the ROI at the peripheral locations and the origin is 8 cm. Fig. 5.20 shows uniformity measurement by manufacturer QA phantom.

5.6.6 Image Noise Measurement

Image noise, defined as

$$\%noise = \frac{\sigma \times CS \times 100}{\mu_w} \qquad [5.3]$$

where σ = standard deviation of CT numbers
CS = contrast scale
μ_w = linear attenuation coefficient of water (~0.192 cm^{-1})

Image noise was determined by using the standard deviation data obtained from homogeneous phantom. The standard deviation of CT no. from the center ROI in phantom image was recorded.

5.6.6.1 Image Noise Measurement by CATPHAN Phantom

Contrast scale in equation 5.3 was used to calculate % noise of CATPHAN phantom. The standard deviation was read from the measurement of image uniformity in module 486 CATPHAN phantom.

5.6.6.2 Image Noise Measurement by Manufacturer QA Phantom

Contrast scale in equation 5.2 was used to calculate % noise of manufacturer QA phantom, material x is a Plexiglas. The standard deviation was read from the measurement of image uniformity in section 3 manufacturer QA phantom.

5.6.7 Low-contrast Resolution Measurement

Low-contrast resolution, defined as the minimum resolvable diameter of an object embedded in a uniform medium that differs in density from its background. It was determined using both phantoms.

5.6.7.1 Low-contrast Resolution Measurement by CATPHAN Phantom

The CATPHAN Module 515 patterns (Fig. 5.22) are clearly seen when the image window and level were adjusted to provide for maximum visibility of all test objects. These settings were approximately window width = 140 and window level = 100 for all scans. The smallest diameters of the test object that can be seen for each % contrast indicate the low-contrast resolution.

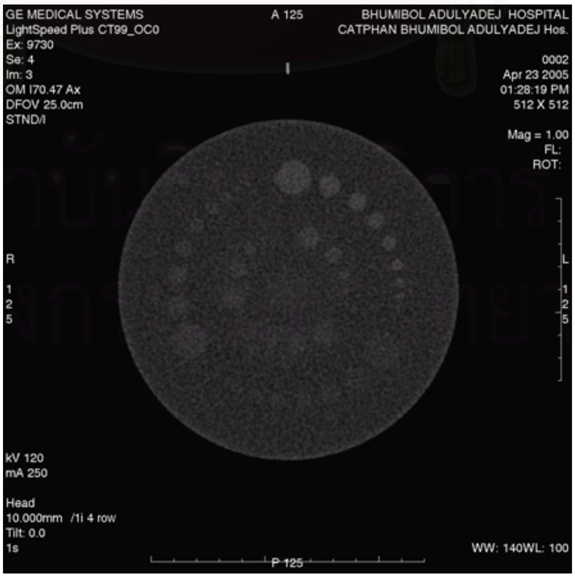

Figure 5.22 Module 515 of CATPHAN phantom for low-contrast detectability

5.6.7.2 Low-contrast Resolution Measurement by Manufacturer QA Phantom

Section 2 (Fig. 5.23) was used to determine the difference of CT number of water and polystyrene and then compare with the Bench Mark values.

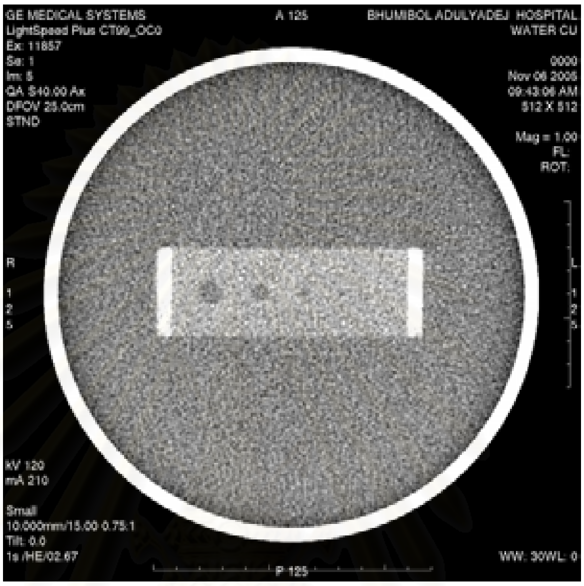

Figure 5.23 Section 2 of manufacturer QA phantom for low-contrast detectability

5.6.8 Limiting High-contrast Resolution Measurement

Limiting high-contrast resolution, defined as the minimum resolvable distance between two high-contrast objects (usually at 5% MTF), was determined using both phantoms.

5.6.8.1 Limiting High-contrast Resolution Measured by CATPHAN Phantom

CATPHAN Module 528 (Fig. 5.24) contains a 0.28mm.diameter tungsten carbide bead. The report pixel value was evaluated to be MTF curve by MATLAB program that was specific created for this work.

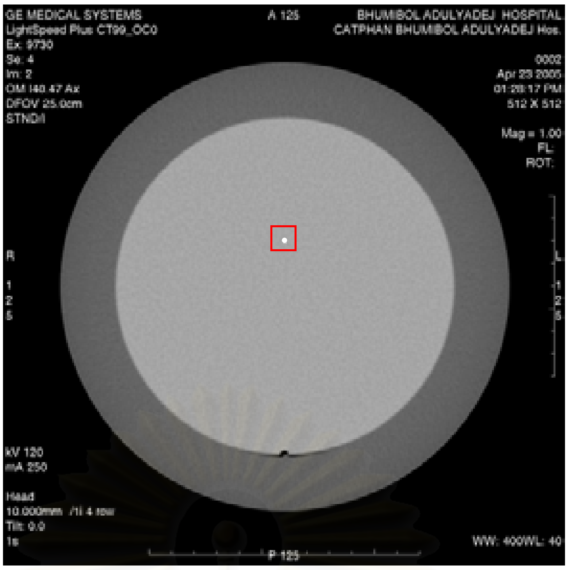

Figure 5.24 Module 528 of CATPHAN phantom with a tungsten carbide bead for MTF calculate

5.6.8.2 Limiting High-contrast Resolution Measured by Manufacturer QA Phantom

Two methods were performed for high contrast resolution measured by manufacturer QA phantom from section 1 (Fig. 5.25). First method was to compare the difference of CT number of water and Plexiglas with the manufacturer recommended values (120 ± 12 HU). And the another method was to compare the standard deviation for a ROI in the 1.6mm bar pattern (the largest bar pattern) with the Bench Mark value.

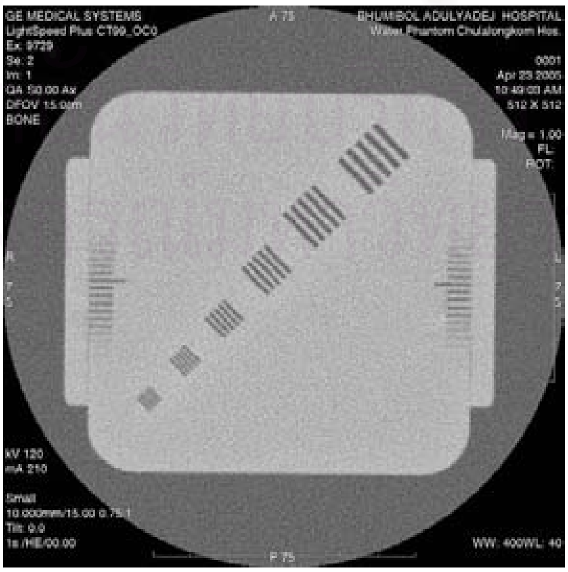

Figure 5.25 Section 1 of manufacturer QA phantom for high contrast resolution

5.6.9 Computed Tomography Dose Index (CTDI) Measurements

Computed tomography dose index (CTDI) measurements were performed according to procedures and dose calculation protocols suggested in the literature [1]. The 10-cm ionization chamber was placed at the center and 4 peripheral locations. Measured values were compared with the manufacturer-specified doses. The manufacturer's acceptability criteria are ±15% from the specified values. CTDI exposure technique factors used in the measurements were the same for the measurements on the LightSpeed Plus® and LightSpeed RT scanners. Exposure techniques used for CTDI measurements were set by the following parameters.

Interface	Input
Entry	Head First
Position	Supine
Anatomical Reference	Head for Head Phantom, Abdomen for Body Phantom
Landmark Location	0 on resolution chamber at circumferential line/cross hatch.
Scan Type	Axial
Slice Thickness	10 mm.
Tilt	0 degrees
SFOV	Small for Head Phantom, Large for Body Phantom
kV	120
mA	250
Rotation speed	1 sec.
DFOV	25 cm for Head Phantom, 50 cm for Body Phantom
Algorithm	Standard
Matrix	512

$CTDI_w$ was evaluated by equation 3.10.

5.7 Data Collection

All measurements are collected in accordance with guidelines set out by the American Association of Physicists in Medicine (AAPM) [1] and the manufacturer suggested [4, 5]. All data were measured 3 times every 2 months to obtain the mean values.

5.8 Data Analysis

We evaluate data by following AAPM Report No.39, AAPM Summer school 1995 [2], AAPM – TG66 Report [3], or manual suggested. Data from 2 scanners are compared within manufacturer tolerances.

5.8.1 The Performance Evaluation Data.

The performance evaluation data is shown in Table 5.4.

Table 5.4 : The performance evaluation data

Measurement	Variables	Analysis	Criteria
CATPHAN			
- Slice thickness	The FWHM length of any of the four wire ramps(FWHM)	$Slice\ thickness\ (mm.) = FWHM \times \tan 23^{\circ}$	Within ±0.5 mm of the slice setting [1]
- CT number accuracy and linearity	The mean CT number of Air, Polystyrene, LDPE, PMP, Teflon, Delrin™, Acrylic.	Plot graph between μ_x (@ 70 keV) and CT number, CS	The CS should be approximately 2.0×10^{-4} cm^{-1}/CT no. [2]
- Image uniformity	The mean CT in ROI at central and peripheral.	Calculate the different of the mean CT no. at center and peripheral	Field uniformity within ±5 HU [1, 2, 3, 15]
- Image noise	The mean CT and SD in ROI at central and peripheral	$\%noise = \frac{\sigma \times CS \times 100}{\mu_w}$ $CS = \frac{1}{slope\ of\ the\ CT\ no.\ vs.\ \mu\ line\ fit}$	% noise less than 0.5 [2]
- Low-contrast resolution	Supra-slice target diameter @ % different contrast, Subslice target diameters @ target length	Follow the definition in CATPHAN Manual	5mm @1% contrast [2, 15]

53

Table 5.4 : The performance evaluation data (Cont.).

Measurement	Variables	Analysis	Criteria
- High-contrast resolution	Pixel values of a 0.28mm diameter tungsten carbide bead	Plot MTF curve by MATLAB program and expressed at a specific cutoff frequency (0.1 or 0.05 are suggested)	Specified at the 5% MTF > 5 lp/cm [2]
Manufacturer-supplied phantom [4, 5]			
- Slice thickness	The number of slice thickness bare	*Slice thickness = The number of slice thickness bare*	Not vary by more than ±1 mm from the expected value
- CT number Accuracy	The mean CT number of water at the central	Follow the definition in Manufacturer Manual	Should see a CT no. for water of ±3 HU for the center ROI
- Image uniformity	The mean CT in ROI at central and peripheral.	Follow the definition in Manufacturer Manual	The uniformity difference between the center ROI and the average of the edge ROIs should be ±3 for small body
- Image noise	SD of CT number within a ROI	Follow criteria of Manufacturer Manual *Image noise = SD of CT number within a ROI* $\%noise = \frac{\sigma \times CS \times 100}{\mu_w}, CS = \frac{\mu_x - \mu_{water}}{CT_x - CT_{water}}$	Standard deviation of the center ROI should equal 3.2 ±0.3 %noise less than 0.5 [2]

Table 5.4 : The performance evaluation data (Cont.).

Measurement	Variables	Analysis	Criteria
- Low-contrast resolution	Water's CT no. and polystyrene membrane's CT no.	Subtraction of polystyrene membrane's CT no. and water's CT no.	Bench Mark values
- High-contrast resolution	Standard deviation for a ROI in the 1.6 mm bar pattern	Follow the definition in Manufacturer Manual	The standard deviation for an ROI in the 1.6 mm bar pattern should equal 37±4 for the standard algorithm
	Plexiglas's CT no. and water's CT no.	Subtraction of Plexiglas's CT no. and water's CT no.	The difference should equal 120±12
Head and body phantom & Ionization chamber DCT 10-RS			
- $CTDI_w$	Absorb dose (cGy) in Head and Body phantom	$CTDI_w = \frac{1}{3}CTDI_{central} + \frac{2}{3}CTDI_{peripheral}$	±15% from the specified values [4]

5.8.2 Data Presentation

The table, line graph, and picture are presented.

5.9 Expected Benefit and Application

This study is designed for the physical performance in image quality and the radiation dose of the large-bore therapeutic CT scanner (LightSpeed RT) at King Chulalongkorn Memorial Hospital when compared with the 70-cm bore diagnostic CT scanner (LightSpeed Plus®) at Bhumibol- adulyadej Hospital. The quality of image from both equipments will allow for the corrected delineation of the tumour and critical organ. The $CTDI_w$ from both scanners were expected to be within the manufacturer suggested 15 % specification. Patient dose received from the CT scan can be evaluated. The manufacturer QA phantom should be available for routine QA after comparison with the CATPHAN phantom.

5.10 Ethic Consideration

As the concerns the study measurement of the physical performance of equipments and radiation dose from phantom, the ethical issues are not necessary.

CHAPTER VI

RESULTS AND DISCUSSION

Before the physical performance for both LightSpeed Plus® and LightSpeed RT scanners were performed, QA of display monitors were checked by SMPTE test pattern and circular symmetry of display system that used CTP 404. Both units render normal display monitors (Fig. 5.15) and circular symmetry display systems. These checks confirmed that the image quality for both scanners were independent on display monitor. In this study, the data were collected 3 times every 2 months. The mean values of three measurements together with standard deviations were calculated. The results could be reported as the followings:

6.1 Slice Thickness Accuracy

The mean measured slice thickness of 1.25-10.0 mm by CATPHAN and manufacturer QA phantoms are shown in Table 6.1. The standard deviations of 3 measurements in CATPHAN phantom for all the slice thickness studied were within 0.22 mm for both units. The 3 measurements in manufacturer QA phantom mostly showed the same reading because it was read by looking the darkness of the lines. The deviations of the measured values from set slice thickness for both scanners are shown in Table 6.2. The results demonstrated that all measured values were within ±0.5 mm criteria with slightly more deviation of LightSpeed Plus® than LightSpeed RT. The maximum deviation from set slice thickness measured by CATPHAN phantom of LightSpeed Plus® was 0.31 mm and LightSpeed RT was 0.24 mm. For manufacturer QA phantom, most of the reading showed less deviation which the maximum deviation was 0.25 mm for both units. The measurements by CATPHAN phantom gave more accurate thickness than manufacturer QA phantom but it was limited by sensitivity of measurement tools and integer value output, so a very thin slice thickness is hard to evaluate and will be get a large error. This study did not evaluate the slice thickness which was less than 1.25 mm. The manufacturer QA method is simply to do but it isn’t delicate. However, it also indicates that the results obtained by the manufacturer QA tests are reliable.

Table 6.1 Slice thickness measured by CATPHAN and manufacturer QA phantoms

Set slice thickness (mm.)	CATPHAN		Manufacturer QA phantom	
	GE LightSpeed Plus®	GE LightSpeed RT	GE LightSpeed Plus®	GE LightSpeed RT
1.25	1.30	1.26	1.00	1.25
2.50	2.49	2.52	2.50	2.50
3.75	3.75	3.64	3.75	3.67
5.00	4.95	4.97	5.00	5.00
7.50	7.32	7.39	Not performed	Not performed
10.00	9.70	9.77	Not performed	Not performed

Table 6.2 Deviation of measured slice thickness from setting values [mm]

Set slice thickness (mm.)	CATPHAN		Manufacturer QA phantom	
	GE LightSpeed Plus®	GE LightSpeed RT	GE LightSpeed Plus®	GE LightSpeed RT
1.25	0.05	0.01	0.25	0.00
2.50	0.01	0.02	0.00	0.00
3.75	0.00	0.11	0.00	0.08
5.00	0.05	0.03	0.00	0.00
7.50	0.18	0.11	Not performed	Not performed
10.00	0.30	0.23	Not performed	Not performed

6.2 CT Number Accuracy and Linearity

The measurements of CT number of various materials were performed by CATPHAN phantom for LightSpeed Plus® and LightSpeed RT, the results are shown in Table 6.3. The readings of 3 times measurements showed consistency with the standard deviation within 0.98 HU. They indicated that the measurements for both scanners were constant and reproducible. Acceptable criteria for air (-1000 ± 3 HU) and water (0 ± 5 HU) has been reported in the literature [2, 3]. The result showed the deviation from nominal CT number of air greater than 3 HU for both scanners because the effect of solid water that fill around an air hole. No standard value was found for other materials. This may be because of the great impact the phantom energy spectrum of a particular x-ray tube has on the measured CT number for a particular material. However, nominal values may be determined using available literature [1, 13]. The literature [2] suggests that even for water, the CT number may change by up to 20 HU, depending on the size of the water phantom used for the scans and the measurement. In this study, the deviation of 20 HU was set as criteria. The deviations of CT number from nominal values of both scanners were comparable and within the criteria, so the effects of large-bore geometry on this image quality parameter seem to be negligible. The mean CT numbers of water and solid water in

CATPHAN for both units shown in Table 6.4 were -0.45 – 0.59 HU and 8.76 – 11.47 HU, respectively. The solid water in CATPHAN ranges 5 – 18 HU [13]. They were within acceptable criteria.

Table 6.3 CT number accuracy and linearity measured by CATPHAN phantom

Material	μ (cm^{-1})	Nominal CT no.	Mean CT no.		Deviation from nominal	
			LightSpeed Plus®	LightSpeed RT	LightSpeed Plus®	LightSpeed RT
Teflon	0.363	990	961.49	962.09	28.51	27.91
Delrin™	0.245	340	355.03	357.15	15.03	17.15
Acrylic	0.215	120	119.90	121.96	0.10	1.96
Polystyrene	0.171	-35	-38.29	-35.82	3.29	0.82
LDPE	0.174	-100	-94.16	-91.74	5.84	8.26
PMP	0.227	-200	-182.45	-179.93	17.55	20.07
Air	0.000	-1000	-979.27	-980.69	20.73	19.31

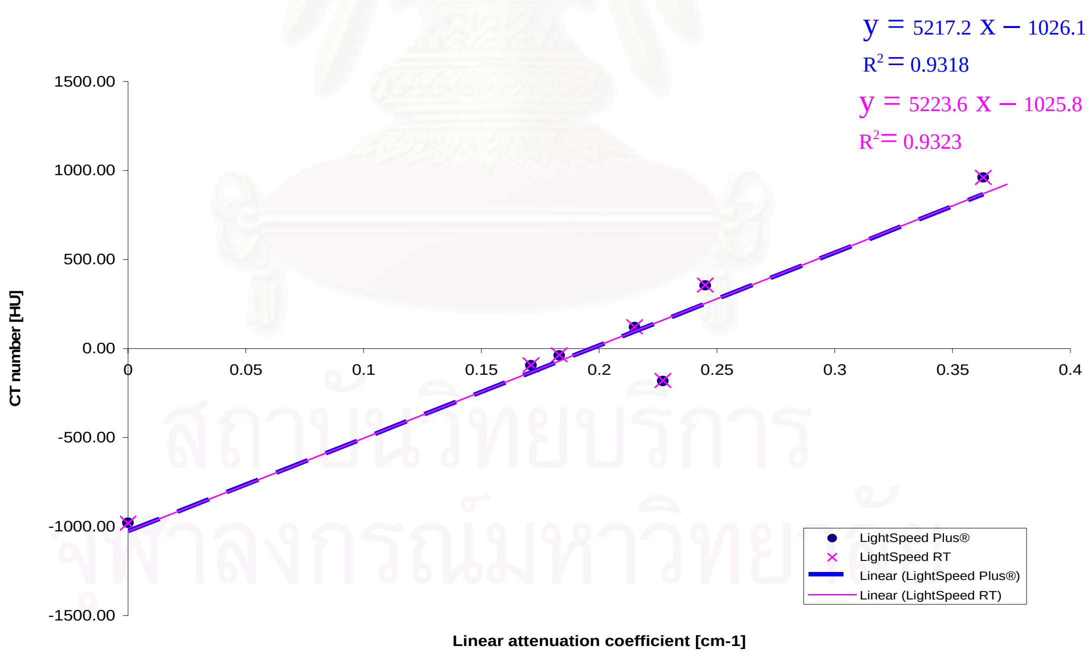

Figure 6.1 Linearity of CT number

The linear relationship between CT number and linear attenuation coefficient, μ (cm^{-1}), from both scanners are shown in Fig. 6.3. Using the expression from equation 5.3 obtained contrast scale of 1.92 $\times 10^{-4}$ and 1.91$\times 10^{-4}$ cm^{-1}/CT no. for the LightSpeed Plus® and LightSpeed RT scanners, respectively. Available literature [2] indicated that within the energy range of 100-140 kVp, the contrast scale (CS) should be approximately 2.0×10^{-4} cm^{-1}/CT no. The contrast scale could be obtained from calculation by the expression in equation 5.2 for manufacturer QA phantom data which is shown in Table 6.8. The values of contrast scale equal 1.91×10^{-4} and 1.90×10^{-4} cm^{-1}/CT no. for LightSpeed Plus® and LightSpeed RT scanners, respectively.

6.3 Uniformity

The manufacturer- specified limit for uniformity in water was 0 ±3 HU for the center ROI and the uniformity different between the center ROI and the average of edge ROIs should be 0 ± 3 HU for small body or 0 ± 10 HU maximum deviations for large body [4]. Published trend specifications [1, 2, 3, 15] were in the order of ±5 HU up to ±10 HU. Table 6.4 shows the CT number at various positions for uniformity measurements. The deviations of mean CT number from the center at various locations are shown in Table 6.5. The deviations were within 0.53 HU for both scanners. Both the manufacturer QA and CATPHAN phantoms gave similar satisfactory result regarding image uniformity for both units.

Table 6.4 Mean CT numbers (HU) at various locations measured by CATPHAN and manufacturer QA phantoms

Location	CATPHAN (Solid water)		Manufacturer QA phantom (Water)	
	GE LightSpeed Plus®	GE LightSpeed RT	GE LightSpeed Plus®	GE LightSpeed RT
Center	9.10	11.47	0.08	0.42
12 o'clock	8.76	11.25	-0.40	0.59
3 o'clock	8.76	11.11	-0.41	0.41
6 o'clock	8.90	11.19	-0.34	0.27
9 o'clock	8.82	11.23	-0.45	0.43

Table 6.5 Deviation of mean CT number (HU) from the center location

Location	CATPHAN (Solid water)		Manufacturer QA phantom (Water)	
	GE LightSpeed Plus®	GE LightSpeed RT	GE LightSpeed Plus®	GE LightSpeed RT
12 o'clock	0.34	0.22	0.50	0.01
3 o'clock	0.34	0.35	0.43	0.15
6 o'clock	0.20	0.28	0.53	0.01
9 o'clock	0.28	0.24	0.48	0.17

6.4 Noise

The standard deviation of pixel values from ROI placed at the center of phantom image and percent image noise based on CATPHAN and manufacturer QA phantoms are shown in Table 6.6. The 900-mm^2-circle-ROI [1] and 400-mm^2-squre-ROI [4, 5] were used for standard deviation measurement by CATPHAN and manufacturer QA phantoms, respectively. The standard deviations of the manufacturer QA phantom data for both scanners were within acceptable tolerance such that the standard deviation in the center of image is 3 ± 0.4 HU. The manufacturer QA phantom data agree with the CATPHAN phantom data, both scanners showed image noise which were within manufacturer specified limits and the typical specifications for diagnostic scanners [2]. Overall, measured noise values were less than 0.5%. The CATPHAN and manufacturer QA phantoms showed slightly lower noise levels of LightSpeed Plus® than LightSpeed RT. The relative decrease in noise from large bore to small bore seems to give an advantage to the small bore.

Table 6.6 Standard deviation and percent image noise measured by CATPHAN and manufacturer QA phantoms

	CATPHAN		Manufacturer QA phantom	
	GE LightSpeed Plus®	GE LightSpeed RT	GE LightSpeed Plus®	GE LightSpeed RT
Center	2.86	3.14	2.82	3.01
*****Noise (%)	0.286	0.313	0.281	0.298

*****Percent noise calculated from equation 5.3.

6.5 Low-contrast Resolution

Data of low-contrast resolution measured by CATPHAN phantom for both scanners are shown in Table 6.7. These results indicated a low-contrast resolution of 8 mm at 0.3% contrast for the LightSpeed Plus® and 9 mm at 0.3% contrast for the LightSpeed RT. These data are agreeable with the noise results of Table 6.6, indicating a slightly improvement in image quality for the small-bore-type scanners. However, the 3mm @ 1% contrast resolution of the 80-cm-bore showed that a unit is still under diagnostically accepted levels of 5 mm @ 1% [2, 15].

Table 6.7 Low-contrast resolution (minimum resolvable diameter [mm]) detected by CATPHAN phantom

Nominal contrast	Supra-slice		Subslice					
	GE LightSpeed Plus®	GE LightSpeed RT	GE LightSpeed Plus®			GE LightSpeed RT		
			*7 mm	*5 mm	*3 mm	*7 mm	*5 mm	*3 mm
1.0%	3	3	5	5	-	5	5	9
0.5%	3	4	-	-	-	-	-	-
0.3%	8	9	-	-	-	-	-	-

*Subslice target length

Table 6.8 Low-contrast resolution (the difference CT numbers between water and polystyrene membrane [HU]) measured by manufacturer QA phantom

Position	Bench Mark Value		Measured value	
	LightSpeed Plus®	LightSpeed RT	LightSpeed Plus®	LightSpeed RT
Above holes	8.13	7.37	7.93	8.24
Below holes	7.97	7.34	7.61	8.15

The data from manufacturer QA phantom is shown in Table 6.8, the contrast which defined by the difference in CT number between water and polystyrene membrane on above and below holes were agreeable according to Bench Mark values within 0.54 HU for both scanners.

6.6 High-contrast Resolution

In this study, the spatial resolution was measured by MTF at the 5% value. It is typically higher than the resolution that can be observed with a line pair. Spatial resolution measured with a line pair phantom may not always meet manufacturer specifications [3]. With this reason and difficulty in reading the line pair, only MTF was used for high contrast resolution measurement in this study. The MTFs were calculated from pixel values that were read from 28 mm diameter tungsten carbide bead in CTP5280, the results are shown in Fig. 6.4 and Table 6.9. Limiting resolution is usually specified at the 5% MTF level with an acceptable limit [2] of higher than 5 lp/cm (1mm). Our measurements indicated a limiting resolution of 7.14 lp/cm for LightSpeed Plus® and 7.29 lp/cm for LightSpeed RT. The LightSpeed RT was slightly superior in term of high contrast resolution. The results agree with noise and low-contrast data, increasing noise and decreasing low-contrast resolution are improving high contrast resolution.

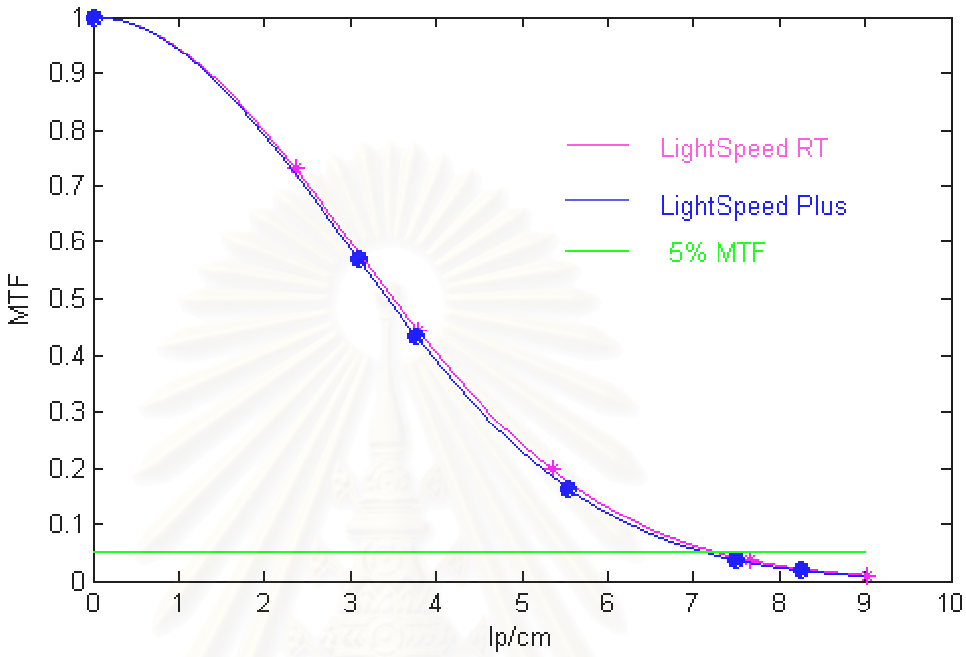

Figure 6.2 Comparative resolutions by MTF between diagnostic and therapeutic CT scanner

Table 6.9 High contrast resolution (lp/cm) measured by CATPHAN phantom

MTF	GE LightSpeed Plus®	GE LightSpeed RT
5%	7.14	7.29
10%	6.26	6.39
20%	5.24	5.34
50%	3.44	3.50

Table 6.10 High contrast resolution (the difference of Plexiglas and water CT numbers [HU]) measured by manufacturer QA phantom

	LightSpeed Plus®	LightSpeed RT
CT number water	0.16	1.02
CT number Plexiglas	120.64	121.94
Difference of CT numbers	120.48	120.92

Table 6.11 High contrast resolution (standard deviation of ROI in the 1.6 mm bar pattern [HU]) measured by manufacturer QA phantom

GE LightSpeed Plus®	GE LightSpeed RT
37.7	37.6

High contrast resolution was tested again by manufacturer QA phantom. There are two methods. The difference in CT number of Plexiglas and water is the one of methods. The results from both units which were within manufacturer acceptable values (120 ± 12 HU) are shown in Table 6.10. Another method is to find the standard deviation of ROI in the 1.6 mm bar pattern for standard algorithm measurement. The results from both units that are shown in Table 6.11 indicated acceptable manufacturer values (37 ± 4 HU).

6.7 Computed Tomography Dose Index

The comparison of measured, auto calculated CTDI values by manufacturer software and ImPACT' s (Imaging Performance Assessment of Computed Tomography, the Department of Health's CT evaluation facility) values for head and body phantoms are shown in Table 6.12 and 6.13, respectively. The measured head CTDI indicated 5.0 and 3.6 cGy at the center and ranged from 4.6 to 5.2 and 3.3 to 4.0 cGy at the peripheral and the measured body CTDI indicated 1.5 and 1.1 cGy at the center and ranged from 3.0 to 3.3 and 1.9 to 2.7 cGy at the peripheral for the 70-cm-bore and 80-cm-bore units, respectively. With these measured CTDI data, $CTDI_w$ was calculated from equation 5.4. $CTDI_w$ of head phantom were 5.0 and 3.7 cGy for LightSpeed Plus® and LightSpeed RT, respectively. $CTDI_w$ of body phantom were 2.6 and 1.9 cGy for LightSpeed Plus® and LightSpeed RT, respectively. The overall agreement of CTDI values is very good. Measured values on the both units were found to be within the manufacturer-suggested 15% specification. CTDI for both phantoms have been reported by the ImPACT [16, 17]. CTDI values on LightSpeed Plus® and LightSpeed RT were agreed with ImPACT's values, they did not exceed than 10%. Head and body doses for the large-bore scanner seem slightly lower compared to LightSpeed Plus®. This may be explained by the fact that it is the effects of the large-bore geometry. The doses agree with noise data, increase noise effected to be higher dose.

Table 6.12 CTDI and $CTDI_w$ (cGy) for head phantom

Phantom position	GE LightSpeed Plus®			GE LightSpeed RT		
	Measured	Calculated	ImPACT [16]	Measured	Calculated	ImPACT [17]
Center	5.0	-	5.3	3.6	-	3.8
Periphery	4.6 – 5.2	-	5.2	3.3 – 4.0	-	4.2
$CTDI_w$	5.0	5.0	3.4	3.7	3.9	4.1

Table 6.13 CTDI and $CTDI_w$ (cGy) for body phantom

Phantom position	GE LightSpeed Plus®			GE LightSpeed RT		
	Measured	Calculated	ImPACT [16]	Measured	Calculated	ImPACT [17]
Center	1.5	-	1.6	1.1	-	1.1
Periphery	3.0 – 3.3	-	3.0	1.9 – 2.7	-	2.6
$CTDI_w$	2.6	2.5	2.5	1.9	2.1	2.1

CHAPTER VII

CONCLUSION

The objective of this study is to compare the physical performance, the image quality and the radiation dose in terms of CTDI in phantom between 70-cm-bore and 80-cm-bore. The same standard protocols were set for both scanners which were produced from the same manufacturer. Manufacturer QA phantom was used to check for the reliability, reproducibility and accuracy by comparing with the CATPHAN phantom. The methods of measurement and criteria were followed AAPM No. 39 [1], AAPM Summer school 1995 [2], AAPM – TG66 Report [3], or manufacturer provided QA protocol. The three times measurements data were collected every 2 months and the mean values were determined. The three times measurement showed less deviation which was demonstrated by small number of standard deviation. Before the image qualities were performed, QA display monitor was checked by SMPTE test pattern which confirmed that the image qualities were independent on display monitor. The same regions of interested size were set in each measurement for parameter controlling. Calculated interpretations were done except low-contrast resolution by CATPHAN phantom, because it does not have another good way to do, so the clearly definition to interpret low-contrast resolution was defined and discussed by four physicists.

The measurement with CATPHAN phantom is the standard tool to compare the characteristics of both scanners. The deviations of the measured slice thickness from the setting for both scanners were within ±0.5 mm which was the standard tolerance. The mean CT number and linearity attenuation coefficient showed linear relationship except PMP. The contrast scales were $1.92\times10^{-4}cm^{-1}$/CT no. for LightSpeed Plus® and $1.91\times10^{-4}cm^{-1}$/CT no. for LightSpeed RT. The standard deviations and image noise of both scanners which represent random error were within manufacturer specified limits and typical specifications for diagnostic scanners. Image noise determines the lower limit of subject contrast that can be distinguished by the observer. The more uniform the background containing a low contrast object, the grater its contrast with that background. Theoretically, minimal noise images should increase normal structure and target delineation accuracy. Noise is a very sensitive parameter to overall imaging performance of the scanner, and can usually be performed in conjunction with uniformity tests. The 80-cm-bore scanner showed relatively small increased in noise compared to 70-cm bore scanner. Image artifacts due to equipment design, beam-hardening, or image reconstruction software can manifest themselves as systemic CT number (HU) variations. Scanning a uniform phantom and sampling mean HU values for ROIs of fixed areas throughout the phantom can quantify the presence of systematic variations. This process is referred to as a field uniformity test. The deviations of CT number at various positions from the center were within 0.35 HU for both scanners. This means less systemic error for both scanners. LightSpeed Plus® showed slightly higher image quality for low-contrast resolutions which were 8 mm at 0.3% contrast compared to 9 mm at 0.3% contrast for LightSpeed RT. For high-contrast resolution, LightSpeed Plus® showed 7.14 lp/cm at 5% MTF level compared to 7.29 lp/cm for LightSpeed RT. The $CTDI_w$ of head phantom for LightSpeed Plus® unit indicated higher dose than LightSpeed RT (5.0 cGy compare to 3.7 cGy). Similarity, the $CTDI_w$ of body phantom for LightSpeed Plus® unit showed higher dose than LightSpeed RT (2.6 cGy compare to 1.9 cGy). This may be due to the effect of the large-bore geometry which the isocenter were placed at longer distance than the small-bore.

All the results showed that LightSpeed RT gave slightly increase high-contrast resolution but slightly decreased in low-contrast resolution so the % noise was higher and radiation dose was low compared with LightSpeed Plus®. High contrast resolution is a fundamental indicator of the scanner's imaging capabilities. The CT-scanners used for CT-simulation should be able to image and differentiate small details in patient anatomy [3]. The measured data indicated that the increased source-to-detector distance (e.g., large-bore configuration) slightly affected the high contrast resolution.

The results from manufacturer QA phantom agree with CATPHAN phantom, manufacturer QA phantom proved to be reliable for routine constancy check and needed to be performed daily for CT number accuracy and image noise [4, 5]. The majority of scanner manufacturers have phantoms and software which can be used to assess image quality as a part of a QA program. Although, the primary purpose of these vendor supplied phantoms is for scanner calibration and automated baseline performance evaluation, it is reasonable to assume that they can be used for periodic scanner performance evaluation. The validity of CT-scanner manufacturer supplied phantoms and software must be verified against independent test methods or phantoms before they can be used for routine QA. During the initial acceptance testing and commissioning, tests should be performed with both, manufacturer phantom and independent test methods. [3]

The measurement of HVL obtained x-ray effective energy of 72 keV which was in the same order as AAPM No. 39 suggestion [1]. At this time, it is difficult to find the standard method for HVL measurement. In the future, standard method to measure HVL should be decided to perform for accurate effective energy and linear attenuation coefficient values chosen. The CT simulator was used for treatment planning so the implementation of tissue inhomogeneity correction in image-based treatment planning will improve the accuracy of radiation dose calculations for patients undergoing external-beam radiotherapy. The proper procedure of establishing the CT value to density conversion relationship should be performed. This tissue characterization relationship allows the conversion of CT value in each voxel of the CT images into density for use in the dose calculations. Further study the relationship between CT value and electron density or physical density suitable for the treatment planning system will improve the accuracy of radiation dose calculation.

In summarizing, for a successful CT-simulation process, the CT-scanner should consistently produce patient images with the highest possible quality and accurate geometrical information. Image quality directly affects the physician's ability to define target volumes and critical structures, and the spatial integrity of the CT study establishes how accurately radiation can be delivered to target volumes. [3]

REFERENCES

1. American Association of Physicist in Medicine. Specification and Acceptance testing of Computed Tomography Scanners, Report 39 (May) 1993.

2. McCollough CH, Zink FE. Quality control and acceptance testing of CT systems. In: Gouldman LW, editor. Medical CT and ultrasound: Current technology and applications. AAPM Summer school 1995.

3. Sasa Mutic, et al. Quality assurance for computed-tomography simulators and the computed-tomography-simulation process: Report of the AAPM Radiation Therapy Committee Task Group No. 66. *Med. Phys.* 2003. 30(10): p. 2762 – 2792.

4. GE Medical Systems. LightSpeed RT Technical Reference Manual. 2003.

5. GE Medical Systems. LightSpeed Plus® Technical Reference Manual. 2000, 2001.

6. Jose L. Garcia-Ramirez, Sasa Mutic, James F. Dempsey, Daniel A. Low, James A. Purdy. Performance evaluation of an 85-cm-bore x-ray computed tomography scanner designed for radiation oncology and comparison with current diagnostic CT scanners. *Int. J. Radiation Oncology Biol. Phys.*, 2002. 52 : p. 1123 – 1131.

7. Cynthia H McCollough, Frank E. Zink. Performance evaluation of a multi-slice CT system. *Med. Phys.* 1999. 26: p. 2223 – 2230.

8. Claire McCann, Hamideh Alasti. Comparative evaluation of image quality from three CT simulation scanners. *Am. Coll. Med. Phys.*, 2004. 5(4): p.55 – 70.

9. Nattawan Jangsri. An evaluation of spatial resolution in computerized tomography. Mahidol University, 1999.

10. Jerrold T. Bushberg, et al. The essential physics of medical imaging. 2nd ed. USA, 2002. : p.255 – 283, p.326 – 372.

11. Dendy PP, Heaton B. Physics for radiologist. Great Britain: Katerprint Typesetting service, 1987.

12. Michael F. McNitt-Gray. Radiation Dose in CT. AAPM/RSNA Physics Tutorial for Residents: Topics in CT. *Radio Graphics*. 2002: p.1541 – 1553.

13. Catphan® 500 Manual. The phantom Laboratory.

14. Scanditronix Wellhöfer. Calibration Protocol for the chamber DCT10-RS Manual.

15. NCRP Rep.99. Quality assurance for diagnostic imaging equipment. 1988.

16. Imaging Performance Assessment of Computed Tomography. Scanners, CTDosimetry. 2000.

17. NHS. Report 06014: Wide bore CT scanner comparison report version 14. February 2006.

18. Modulation Transfer Function of a Digital Camera System using an Implementation of the Edge Technique, MSc Digital Imaging-Image Quality Module. February 16, 1999.

19. The Scientist and Engineer's Guide to Digital Signal Processing. Special Imaging Techniques: p. 423 – 450.

APPENDIX

APPENDIX I

The process to estimate of the 2D spatial frequency response characteristics of the CT system (MTF)

Suppose we want to compare two imaging systems, with the goal of determining which has the best spatial resolution. In other words, we want to know which system can detect the smallest object. One way to measure image resolution is by looking at the frequency response. The line pair gauge measurement which is a common method is used. A strong advantage of this method is that it is simple and fast. The strongest disadvantage is that it relies on the human eye, and therefore has a certain subjective component. Another method that can eliminate these problems is the FFT method. In imaging jargon, this display of the frequency response is called the Modulation Transfer Function (MTF). Because of this method should be taking the Fourier transform of the PSF, so it very difficult in practice. Therefore the MATLAB program is used to easier determine the FFT method. In this research, the program was specially created by the thesis owner. The process is explained below [1, 4, 13, 18, 19].

- A CTP528 which is one of four sections of Catphan®500 which has a 0.28 mm diameter tungsten carbide bead was scanned. A 25-cm. DFOV was set.

- Use the impulse source to estimate the point source response function of the CT system. Print out a digitized image of the area surrounding the impulse source. Use the numerical data to determine the two-dimensional array of the CT values arising from the impulse source.

	210	211	212	213	214	215	216	217	218	219	220
252	90	94	99	100	94	84	88	97	99	97	97
253	84	93	100	95	88	86	94	104	106	100	100
254	90	96	97	100	129	145	119	98	100	99	96
255	93	97	94	137	252	304	208	110	94	99	99
256	92	97	100	168	330	397	265	118	87	95	95
257	89	96	99	138	242	287	196	99	84	93	89
258	91	96	98	100	122	134	106	84	91	96	92
259	90	89	92	92	91	92	89	95	102	99	97
260	91	86	88	97	102	100	95	100	101	95	93
261	98	94	93	99	102	98	93	98	102	96	89
262	105	99	96	100	101	94	92	99	105	103	93

- The CT number background is calculated by average peripheral CT values.

	210	211	212	213	214	215	216	217	218	219	220
252	**90**	**94**	**99**	**100**	**94**	**84**	**88**	**97**	**99**	**97**	**97**
253	**84**	93	100	95	88	86	94	104	106	100	**100**
254	**90**	96	97	100	129	145	119	98	100	99	**96**
255	**93**	97	94	137	252	304	208	110	94	99	**99**
256	**92**	97	100	168	330	397	265	118	87	95	**95**
257	**89**	96	99	138	242	287	196	99	84	93	**89**
258	**91**	96	98	100	122	134	106	84	91	96	**92**
259	**90**	89	92	92	91	92	89	95	102	99	**97**
260	**91**	86	88	97	102	100	95	100	101	95	**93**
261	**98**	94	93	99	102	98	93	98	102	96	**89**
262	**105**	**99**	**96**	**100**	**101**	**94**	**92**	**99**	**105**	**103**	**93**

- Net CT number is evaluated by this equation :

$$Net\ CT\ no. = measured\ CT\ no. - Background\ CT\ no.$$

The two-dimensional array of the net CT values is called point spread function (PSF).

-5	-1	4	5	-1	-11	-7	2	4	2	2
-11	-2	5	0	-7	-9	-1	9	11	5	5
-5	1	2	5	34	50	24	3	5	4	1
-2	2	-1	42	157	209	113	15	-1	4	4
-3	2	5	73	235	302	170	23	-8	0	0
-6	1	4	43	147	192	101	4	-11	-2	-6
-4	1	3	5	27	39	11	-11	-4	1	-3
-5	-6	-3	-3	-4	-3	-6	0	7	4	2
-4	-9	-7	2	7	5	0	5	6	0	-2
3	-1	-2	4	7	3	-2	3	7	1	-6
10	4	1	5	6	-1	-3	4	10	8	-2

- The line spread function is defined as distribution of absorbed energy per unit area in the image plane when the imaging system is irradiated by an infinitely long, vanishingly narrow slit. The line spread function is composed of overlapping point spread functions. So summing the columns (y axis) of net CT numbers in the PSF, the line spread function (LSF) for the x axis is obtained.

-5	-1	4	5	-1	-11	-7	2	4	2	2
-11	-2	5	0	-7	-9	-1	9	11	5	5
-5	1	2	5	34	50	24	3	5	4	1
-2	2	-1	42	157	209	113	15	-1	4	4
-3	2	5	73	235	302	170	23	-8	0	0
-6	1	4	43	147	192	101	4	-11	-2	-6
-4	1	3	5	27	39	11	-11	-4	1	-3
-5	-6	-3	-3	-4	-3	-6	0	7	4	2
-4	-9	-7	2	7	5	0	5	6	0	-2
3	-1	-2	4	7	3	-2	3	7	1	-6
10	4	1	5	6	-1	-3	4	10	8	-2

-30	-6	13	183	610	778	402	59	28	29	-3

- Plot a curve between normalized net CT number or relative CT number and distance from middle pixel. A distance between closed pixels is calculated by this equation :

$$distance = \frac{DFOV}{Matrix\ size}$$

when *DFOV* is a display field of view setting (25cm.)
and *Matrix size* is the row or column of the pixel array which forms the displayed CT image (512×512). The curve is called profile of the impulse source.

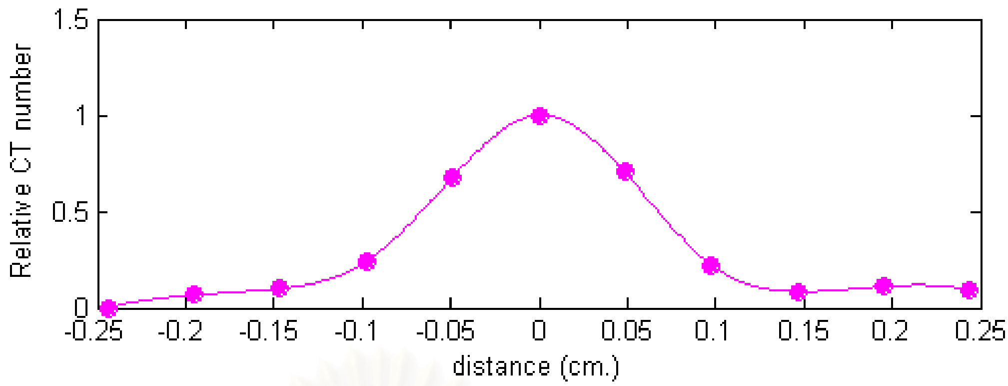

- Full Width at Half Maximum (FWHM) is calculated from the above profile.

- Two group of the LSF was divided by midline of the profile. One group was considered.

- Take the modulus to the Fourier Transform of the LSF elements. Normalize the MTF data with respect to the DC component.

$$MTF = \frac{|H_{\omega_x}|}{H(0)}$$

when H_{ω_x} is the Fourier Transform of a LSF element on *x* position.

$H(0)$ is the DC component or the maximum absolute Fourier Transform of all LSF elements

- Plotting a graph between spatial frequency (lp/cm.) and MTF, when the frequency (υ) is obtained by this equation :

$$\upsilon = \frac{1.665}{FWHM} \times \frac{\sqrt{-\ln MTF(\upsilon)}}{\pi}$$

VITAE

NAME	Miss. Nonlapas Wongwaen
SEX	Female
NATIONALITY	Thai
DATE OF BIRTH	15 August 1977
PLACE OF BIRTH	Prachuapkhirikhan Province, Thailand
INSTITUTIONS ATTENDED	Chulalongkorn University, 2000 : Bachelor of Science (Mathematics)
	Chulalongkorn University, 2006 : Master of Science (Medical Imaging)
HOME ADDRESS	41/343 Soi. Intamara 29 Sutthisarnvinitchai Road Samsennai Phayathai Bangkok Thailand 10400 Tel. 02-616-0280